

NANOG alone induces germ cells in primed epiblast *in vitro* by activation of enhancers

Kazuhiro Murakami^{1,2,3,4,5*}, Ufuk Günesdogan^{1,2,3*}, Jan J. Zylicz^{1,2,3}, Walfred W. C. Tang^{1,2,3},
Roopsha Sengupta^{1,2,3}, Toshihiro Kobayashi^{1,2,3}, Shinseog Kim^{1,2,3}, Richard Butler¹, Sabine
Dietmann³, M. Azim Surani^{1,2,3}

¹Wellcome Trust/Cancer Research UK Gurdon Institute, University of Cambridge, Tennis Court Road, Cambridge CB2 1QN, UK.

²Department of Physiology, Development and Neuroscience, University of Cambridge, Downing Street, Cambridge CB2 3DY, UK.

³Wellcome Trust Medical Research Council Stem Cell Institute, University of Cambridge, Tennis Court Road, Cambridge CB2 1QR, UK.

⁴Laboratory for Pluripotent Cell Studies, Center for Developmental Biology, RIKEN, 2-2-3 Minatojima-minamimachi, Chuo-ku, Kobe, Hyogo 650-0047, Japan.

⁵Laboratory for Molecular and Cellular Biology, Faculty of Advanced Life Science, Hokkaido University, Kita21 Nishi11, Kita-ku, Sapporo, Hokkaido 001-0021, Japan.

*These authors contributed equally to this work.

Correspondence: a.surani@gurdon.cam.ac.uk

Nanog, a core pluripotency factor in the inner cell mass of blastocysts, is also expressed in unipotent primordial germ cells (PGC) in mice¹, where its precise role is yet unclear²⁻⁴. We investigated this in an *in vitro* model, where naïve pluripotent embryonic stem cells (ESCs) cultured in bFGF/ActivinA develop as epiblast-like cells (EpiLCs), and gain competence for PGC-like fate⁵. Consequently, bone morphogenetic protein (BMP4), or ectopic expression of key germline transcription factors *Prdm1/ Prdm14/ Tfp2c*, directly induce PGC-like cells (PGCLCs) in EpiLCs, but not in ESCs⁶⁻⁸. Here we report an unexpected discovery that *Nanog* alone can induce PGCLCs in EpiLCs, independently of BMP4. We propose that following the dissolution of the naïve ESC pluripotency network during establishment of EpiLCs^{9,10}, the epigenome is reset for cell fate determination. Indeed, we found genome-wide changes in NANOG binding pattern between ESCs and EpiLCs, indicating epigenetic resetting of regulatory elements. Accordingly, we show that NANOG can bind and activate enhancers of *Prdm1* and *Prdm14* in EpiLCs *in vitro*; BLIMP1 (encoded by *Prdm1*) then directly induces *Tfp2c*. Furthermore, while SOX2 and NANOG promote the pluripotent state in ESCs, they show contrasting roles in EpiLCs since *Sox2* specifically represses PGCLC induction by *Nanog*. This study demonstrates a broadly applicable mechanistic principle for how cells acquire competence for cell fate determination, resulting in the context-dependent roles of key transcription factors during development.

Transcription factors and epigenetic changes confer competence for somatic and PGC fates when naïve pluripotent inner cell mass (ICM) from embryonic day (E) 3.5-4.5 blastocysts develop to primed epiblast at ~E 6.0¹¹. Similarly, naïve pluripotent embryonic stem cells (ESCs) in '2i' acquire competency within ~48h following culture in bFGF/ActivinA *in vitro*, when day 2 epiblast-like cells (D2 EpiLCs) differentiate into PGC-like cells (PGCLCs) in response to BMP4⁵. These putative PGCLCs show expression of $\Delta PE-Oct4$ -GFP (hereafter called GOF-GFP) and *Blimp1*-GFP reporters (**Fig. 1a and Extended Data Fig. 1a-c**), following upregulation of the three key regulators of PGCLCs; *Prdm1* (encoding BLIMP1), *Prdm14* and *Tfap2c* (encoding AP2 γ)^{5,7,8}.

NANOG and PRDM14 share similar binding profiles in ESCs and contribute to pluripotency¹². While *Prdm14* is also a key regulator of PGC fate^{13,14}, the role of *Nanog* is unclear, although *Nanog* is detected in E6.5 posterior proximal epiblast^{15,16}, the site of PGC induction, and thereafter in the early germline^{1,7}. However, we unexpectedly found that Doxycycline (Dox) induced expression of *Nanog* alone, stimulated GOF-GFP and *Blimp1*-GFP expression in D2 EpiLCs, indicating specification of putative PGCLCs (**Fig. 1a, Extended Data Fig. 1a, d-f, 2a-e**). Furthermore, *Nanog* apparently acts synergistically with BMP4 to increase the number of GFP+ve cells, which we did not see with *Oct4* (**Extended Data Fig. 2f-h**). *Nanog* induced PGCLCs in the presence of Noggin, a BMP signalling inhibitor, demonstrating that it acts independently of BMP-SMAD signalling (**Fig. 1b**). Physiological (equivalent to ESCs) or higher levels of NANOG induced PGCLCs with similar efficiency (**Extended Data Fig. 3a-c**).

We analysed FACS-sorted *Nanog*-induced GFP+ve cells, which showed upregulation of the key PGC regulators; *Prdm1/Prdm14/Tfap2c* as well as *Nanos3* and *Dppa3*, but ESC-specific *Klf4* was downregulated (**Fig. 1c, Extended Data Fig. 3d-f**). This mirrors the response seen with BMP4-mediated PGCLC induction⁵. Notably, PCA analysis of global gene expression confirmed that *Nanog*- and BMP4-induced D4 PGCLCs are highly similar, and closely match with the previously reported D6 PGCLCs⁵ (**Fig. 1d, Extended Data Fig. 3g-j**). Further, BLIMP1, PRDM14 and AP2 γ (but not KLF4) were detected in PGCLCs by immunofluorescence (IF) (**Fig. 1e, Extended Data Fig. 4**). Thus, *Nanog* clearly induces PGC-like fate in EpiLCs and not their reversion to ESCs.

The *Nanog*-induced PGCLCs also showed unique early germline-specific epigenetic modifications; global enrichment of H3K27me3 and erasure of H3K9me2^{17,18} (**Fig. 1e, Extended Data Fig. 4**), together with the initiation of DNA demethylation through the repression of *Uhrf1*, *Dnmt3a* and *Dnmt3b* (**Fig. 1c, Extended Data Fig. 3e, i**), and upregulation of 5-hydroxymethylcytosine (5hmC) and TET1¹⁹ (**Extended Data Fig. 4**). Expression of *Dazl* also indicated progression of DNA demethylation in PGCLCs (**Extended Data Fig. 4a, b**), which is reminiscent of BMP4-induced PGCLCs⁵.

Next, we asked if *Nanog*- and cytokine-induced PGCLCs could dedifferentiate into pluripotent embryonic germ cells (EGCs) as seen with E8.5 PGCs¹¹. We first subjected PGCLCs to a selection with retinoic acid and bFGF for 5 days, which promotes PGCLC proliferation, but not of ESC-like cells^{20,21} (**Extended Data Fig. 5a, b**). The resulting PGCLCs were transferred to 2i/LIF to promote their dedifferentiation into EGC-like cells (EGCLCs), which after several passages produced self-renewing GFP+ve EGCLCs (**Extended Data Fig. 5b**). These EGCLCs when introduced into blastocysts contributed extensively (in 27/29 embryos) to chimeric fetuses at E9.5 (**Extended Data Fig. 5c**), unlike 'unipotent' PGCLCs/PGCs, which neither integrated nor contributed to the fetus (**Extended Data Fig. 5d-g**).

We then sought genetic evidence that *Nanog* induces *bona fide* PGCLCs using ESCs with a mutation in *Prdm1*, which is obligatory for PGC specification, but not for the pluripotent state^{22,23}. Consistently, no PGCLCs were induced from *Prdm1*^{-/-} D2 EpiLCs, nor did they revert to ESCs (**Fig. 2a, Extended Data Fig. 6a, b**). Instead, the aggregates showed somatic gene expression, including *Hoxa1* and *Hoxb1*, which is reminiscent of the aborted PGC fate in *Prdm1*^{-/-} embryos *in vivo*²². Furthermore, H3S10ph and γ H2A.X analysis by IF of D6 aggregates indicated that while cell proliferation was unaffected, the rate of apoptosis increased, presumably as the differentiated cells could not survive in the culture conditions (**Extended Data Fig. 6c, d**).

To further investigate PGCLC induction by *Nanog*, we generated CRISPR/Cas9-mediated *Nanog*

knockout alleles in GOF-GFP ESCs with Dox-inducible *Nanog* (**Fig. 2b, c**). We found a significant reduction in the induction of PGCLCs from *Nanog* mutant cells in response to BMP4 (**Fig. 2d-f**), but ectopic *Nanog* expression rescued this deficit, suggesting complementary roles for BMP4 and *Nanog* in PGCLC induction.

Next, we investigated if the Wnt-BRACHYURY pathway is important for PGCLC induction by *Nanog* as is the case with BMP4²⁴. We induced PGCLCs in the presence of XAV939 tankyrase inhibitor, which promotes degradation of β -catenin²⁵ resulting in the repression of *Brachyury* (**Extended Data Fig. 6e-g**). PGCLC induction with BMP4 was repressed by XAV939 but not when induced with *Nanog* (**Extended Data Fig. 6h, i**). Furthermore, Wnt had no detectable effect on *Nanog* expression (**Extended Data Fig. 6g, i**), indicating that *Nanog* acts independently of Wnt-BRACHYURY.

We then asked when during the transition of ESCs to EpiLCs, cells become responsive to *Nanog* for PGCLC induction. We found a large majority of D1 EpiLCs (63.8%) reverted to ESCs when transferred to 2i/LIF medium, and *Nanog* enhanced this response (to 84.7%), as confirmed by expression of *Klf4* and repression of PGC genes (**Fig. 3a-c**). This reversion to ESCs diminished significantly in D2 EpiLCs (28.4%), and *Nanog* repressed it further (to 9.8%); instead these cells exhibited a distinct phenotype with expression of *Brachyury* and *Wnt3* mesodermal genes (**Fig. 3a-c**). Thus, D2 EpiLCs do not revert to ESCs but acquire competence for PGCLC fate in response to *Nanog*.

Nanog and *Sox2* promote pluripotency in ICM, but thereafter *Nanog* is detected in the E6.25 posterior epiblast where PGCs arise^{15,16}, and *Sox2* in the anterior epiblast where it promotes neuronal fate and inhibits mesodermal specification¹⁶. *Sox2* also represses germline genes in ESCs²⁶ (**Extended Data Fig. 7a**). We tested their roles in our experimental model using ESCs with Dexamethasone (Dex)-inducible knockout of *Sox2*²⁷, in conjunction with Dox-inducible *Nanog* (**Fig. 3d, Extended Data Fig. 7b**). Loss of *Sox2* caused a moderate upregulation of *Prdm1/Tfp2c* in ESCs without affecting *Nanog* expression (**Extended Data Fig. 7c, d**). Notably, *Nanog* induced

Prdm1/Prdm14/Tfap2c in *Sox2* knockout D1 EpiLCs but not in wildtype cells (**Fig. 3e, Extended Data Fig. 7e**). Since there is a gradual decline in *Sox2* during development of EpiLCs⁵ (**Extended Data Fig. 7d**), residual *Sox2* in D1 EpiLCs might repress competency for PGCLCs, and accounts for their reversion to ESCs in response to *Nanog* (**Fig. 3a-c**). By contrast, Dox-induced expression of *Sox2* strongly repressed PGCLC specification in D2 EpiLCs in response to *Nanog* but not BMP4 (**Fig. 3f, Extended Data Fig. 7f-i**). *Sox2* however caused rapid proliferation of PGCLCs *after* their induction by BMP4 (**Extended Data Fig. 8**), consistent with its role in PGCs *in vivo*²⁸. Thus, progressive downregulation of *Sox2* in EpiLCs contributes to competency for PGCLCs, but thereafter *Sox2* supports proliferation of early germ cells. This further confirms that *Nanog* and BMP-SMAD act independently during PGCLC induction.

While both *Nanog* and BMP4 induce PGCLCs, the temporal sequence of *Prdm1/Prdm14/Tfap2c* induction differs slightly. *Nanog* induces *Prdm14* first at 3h, that increases rapidly over ~18h (**Fig. 4a**). This is followed by *Prdm1* at ~12h that increases over the following 12h, and finally *Tfap2c* expression at ~18h. Thus, all the three regulators of PGCLCs are upregulated within ~24h. While the response of D2 EpiLCs to BMP4 is similar, *Prdm1* expression is detected first and slightly ahead of *Tfap2c*, followed by *Prdm14* (**Extended Data Fig. 9a**). *Tfap2c*, a direct target of BLIMP1^{7,8}, is rapidly induced by *Prdm1* alone within 6h (**Extended Data Fig. 9b**).

To explore how NANOG promotes both pluripotency and the induction of PGCLCs, we performed NANOG ChIP-seq in ESCs and 3h after induction of physiological levels (equivalent to ESCs) of NANOG in EpiLCs (**Extended Data Fig. 9c**). We found NANOG binding primarily in the intergenic regions and introns (>90%), where enhancer elements reside (**Fig. 4b, Extended Data Fig. 9d**), with marked differences in binding patterns and enriched motifs in ESCs compared to EpiLCs (**Fig. 4c, Extended Data Fig. 9e**); this provides a basis for the context-dependent functions of NANOG. Overall, many D2 EpiLC enhancers bound by NANOG show enrichment of H3K27ac in D2 PGCLCs, indicative of active enhancers²⁹ (**Extended Data Fig. 9f-h**). This shows that during PGCLC induction, NANOG might contribute to the activation of these elements together with BLIMP1/PRDM14/AP2 γ . Importantly, we also found and confirmed intergenic NANOG binding

sites proximate to the *Prdm14* and *Prdm1* loci (**Fig. 4d, Extended Data Fig. 10a, b**). These sites were devoid of the promoter and gene-body associated H3K4me3 and H3K36me3 modifications, respectively. Instead, they were enriched for the enhancer associated H3K4me1 modification in EpiLCs, suggesting their priming before activation via NANOG and gain of H3K27ac in PGCLCs (**Fig. 4d, Extended Data Fig. 10a**). Since *Prdm14* is critical for both ESCs and PGCLCs, its enhancer showed a similar H3K4me1/H3K27ac/NANOG enrichment profile in both cell types.

Next, we tested the putative *Prdm1* enhancer in luciferase reporter assay, and found that following its low activity in ESCs and EpiLCs, *Nanog* activated the enhancer within 24h after PGCLC induction (**Fig. 4e, Extended Data Fig. 10c, d**). Notably, *Sox2* strongly repressed this activity consistent with SOX2 binding to this enhancer (**Fig. 4e, f, Extended Data Fig. 10c, d**). By contrast, the putative *Prdm14* enhancer, which did not bind SOX2 (**Fig. 4f**), was active in ESCs; this declined in EpiLCs but increased again within 12h after the induction of PGCLCs by *Nanog* (**Fig. 4g, Extended Data Fig. 10c, e**). This reflects the importance of *Prdm14* for both pluripotency and PGCLC fate. Notably, while both BRACHYURY and NANOG bind to and activate the *Prdm1* enhancer²⁴, the latter acts independently of Wnt during PGCLC induction (**Fig. 4e, Extended Data Fig. 6e-i and 10c, d**). Thus, NANOG activates key regulators of PGCLCs independently of BMP4 and Wnt signalling. Additional regulatory elements associated with *Prdm1/Prdm14* may respond similarly.

In conclusion, the resetting of the epigenome during the gain of competency for PGC-like fate is reflected in the differential NANOG binding pattern in ESCs and EpiLCs, consistent with its role in pluripotency and PGCLC specification (**Extended Data Fig. 10f**). *Nanog* is detected in the proximal epiblast and the early germline^{15,16}. Transcription factors also affect competency, since SOX2 inhibits the induction of PGCLCs by NANOG, while NANOG and SOX2 cooperatively promote pluripotency in the ICM/ESCs. NANOG acts independently of BMP4 during PGCLC induction, but they might act cooperatively *in vivo*, since loss of *Nanog* significantly impairs the efficiency of PGCLC specification *via* BMP4. Notably, epigenome resetting during differentiation of competent EpiLCs establishes a mechanistic paradigm for context-dependent roles of transcription

factors such as NANOG that could apply generally during development.

References

1. Yamaguchi, S., Kimura, H., Tada, M., Nakatsuji, N. & Tada, T. Nanog expression in mouse germ cell development. *Gene Expr. Patterns* **5**, 639–646 (2005).
2. Chambers, I. *et al.* Nanog safeguards pluripotency and mediates germline development. *Nature* **450**, 1230–1234 (2007).
3. Yamaguchi, S. *et al.* Conditional knockdown of Nanog induces apoptotic cell death in mouse migrating primordial germ cells. *Development* **136**, 4011–4020 (2009).
4. Carter, A. C., Davis-Dusenbery, B. N., Koszka, K., Ichida, J. K. & Eggan, K. Nanog-independent reprogramming to iPSCs with canonical factors. *Stem Cell Reports* **2**, 119–126 (2014).
5. Hayashi, K., Ohta, H., Kurimoto, K., Aramaki, S. & Saitou, M. Reconstitution of the mouse germ cell specification pathway in culture by pluripotent stem cells. *Cell* **146**, 519–532 (2011).
6. Lawson, K. A. *et al.* Bmp4 is required for the generation of primordial germ cells in the mouse embryo. *Genes Dev.* **13**, 424–436 (1999).
7. Magnúsdóttir, E. *et al.* A tripartite transcription factor network regulates primordial germ cell specification in mice. *Nat. Cell Biol.* **15**, 905–915 (2013).
8. Nakaki, F. *et al.* Induction of mouse germ-cell fate by transcription factors in vitro. *Nature* **501**, 222–226 (2013).
9. Buecker, C. *et al.* Reorganization of enhancer patterns in transition from naive to primed pluripotency. *Cell Stem Cell* **14**, 838–853 (2014).
10. Zyllicz, J. J. *et al.* Chromatin dynamics and the role of G9a in gene regulation and enhancer silencing during early mouse development. *eLife*, 10.7554/eLife.09571 (2015).
11. Surani, M. A., Hayashi, K. & Hajkova, P. Genetic and epigenetic regulators of pluripotency. *Cell* **128**, 747–762 (2007).
12. Ma, Z., Swigut, T., Valouev, A., Rada-Iglesias, A. & Wysocka, J. Sequence-specific regulator Prdm14 safeguards mouse ESCs from entering extraembryonic endoderm fates. *Nat. Struct. Mol. Biol.* **18**, 120–127 (2011).
13. Yamaji, M. *et al.* Critical function of Prdm14 for the establishment of the germ cell lineage in mice. *Nat. Genet.* **40**, 1016–1022 (2008).
14. Grabole, N. *et al.* Prdm14 promotes germline fate and naive pluripotency by repressing FGF signalling and DNA methylation. *EMBO Rep.* **14**, 629–637 (2013).
15. Sun, L. T. *et al.* Nanog co-regulated by Nodal/Smad2 and Oct4 is required for pluripotency in developing mouse epiblast. *Dev. Biol.* **392**, 182–192 (2014).
16. Hoffman, J. A., Wu, C. I. & Merrill, B. J. Tcf711 prepares epiblast cells in the gastrulating mouse embryo for lineage specification. *Development* **140**, 1665–1675 (2013).
17. Seki, Y. *et al.* Extensive and orderly reprogramming of genome-wide chromatin modifications associated with specification and early development of germ cells in mice. *Dev. Biol.* **278**, 440–458 (2005).
18. Hajkova, P. *et al.* Chromatin dynamics during epigenetic reprogramming in the mouse germ line. *Nature* **452**, 877–881 (2008).
19. Hackett, J. A. *et al.* Germline DNA demethylation dynamics and imprint erasure through 5-hydroxymethylcytosine. *Science* **339**, 448–452 (2013).
20. Koshimizu, U., Watanabe, M. & Nakatsuji, N. Retinoic acid is a potent growth activator of mouse primordial germ cells in vitro. *Dev. Biol.* **168**, 683–685 (1995).
21. West, J. A. *et al.* A role for Lin28 in primordial germ-cell development and germ-cell malignancy. *Nature* **460**, 909–913 (2009).
22. Ohinata, Y. *et al.* Blimp1 is a critical determinant of the germ cell lineage in mice. *Nature* **436**, 207–213 (2005).
23. Bao, S. *et al.* The germ cell determinant Blimp1 is not required for derivation of pluripotent stem cells. *Cell Stem Cell* **11**, 110–117 (2012).
24. Aramaki, S. *et al.* A mesodermal factor, T, specifies mouse germ cell fate by directly

- activating germline determinants. *Dev. Cell* **27**, 516–529 (2013).
25. Huang, S.-M. A. *et al.* Tankyrase inhibition stabilizes axin and antagonizes Wnt signalling. *Nature* **461**, 614–620 (2009).
 26. Adachi, K. *et al.* Context-dependent wiring of Sox2 regulatory networks for self-renewal of embryonic and trophoblast stem cells. *Mol. Cell* **52**, 380–392 (2013).
 27. Masui, S. *et al.* Pluripotency governed by Sox2 via regulation of Oct3/4 expression in mouse embryonic stem cells. *Nat. Cell Biol.* **9**, 625–635 (2007).
 28. Campolo, F. *et al.* Essential role of Sox2 for the establishment and maintenance of the germ cell line. *Stem Cells* **31**, 1408–1421 (2013).
 29. Creyghton, M. P. *et al.* Histone H3K27ac separates active from poised enhancers and predicts developmental state. *Proc. Natl. Acad. Sci. U.S.A.* **107**, 21931–21936 (2010).
 30. Kurimoto, K. *et al.* Quantitative Dynamics of Chromatin Remodeling during Germ Cell Specification from Mouse Embryonic Stem Cells. *Cell Stem Cell* **16**, 517–532 (2015).
-

Supplementary Information is linked to the online version of the paper at www.nature.com/nature.

Acknowledgements

We thank Harry Leitch for ESC lines, Caroline Lee for help with animal husbandry, Hitoshi Niwa for vectors and conditional Sox2-KO ESCs, Nigel Miller, Rachel Walker and Andy Riddell for FACS sorting and Julien Bauer for analysis of microarray data. K.M. was supported by the JSPS Institutional Program for Young Researchers Overseas Visits. U.G. was supported by a Marie Skłodowska-Curie and a Newton Trust/Leverhulme Trust Early Career fellowship. J.J.Z. was a recipient of a Wellcome Trust PhD Studentship (RG44593). T.K. was supported by a JSPS Fellowship for research abroad. This research was supported by Gurdon Institute core grants from the Wellcome Trust (092096) and the Cancer Research UK (C6946/A14492) and a grant from the Wellcome Trust to M.A.S. (WT096738).

Author contribution

K.M. and U.G. designed and performed experiments, and wrote the paper; W.T. designed and carried out the luciferase assays; NANOG ChIP experiments were carried out by J.J.Z., while R.S. performed immunofluorescence analysis; T.K. and S.K. designed and carried out the chimera experiments; S.D. performed bioinformatic analysis; R.B. developed the ‘Object Scan’ plugin; M.A.S. supervised the project, designed experiments and wrote the paper. All authors discussed the results and contributed to the manuscript.

Author information

The accession number for the microarray data presented in this study is available from the Gene Expression Omnibus (GEO) database under accession GSE71933. Reprints and permissions information is available at www.nature.com/reprints. The authors declare no competing financial interests. Readers are welcome to comment on the online version of the paper. Correspondence and requests for materials should be addressed to M.A.S. (a.surani@gurdon.cam.ac.uk).

Figure Legends

Figure 1: *Nanog* induces PGCLCs in EpiLCs.

- a**, Brightfield/GFP representing D4 male PGCLCs induced by *Nanog* (+Dox); % GFP+ve cells after FACS; scale bar, 200 μ m.
- b**, FACS plots for GOF-GFP+ve D4 PGCLCs induced by BMP4 or *Nanog* (+Dox) and +/-Noggin.
- c**, Analysis of male GOF-GFP cells (qPCR) as indicated. GFP+ve cells were FACS sorted. $\Delta\Delta$ Ct +/- s.d. (n=3 biological replicates).
- d**, Microarray analyses of GOF-GFP ESCs and PGCLCs; unsupervised hierarchical clustering, and principal component (PC)1 scores.
- e**, IF of *Nanog*-induced BLIMP1-GFP+ve PGCLCs. Arrowheads highlight single GFP+ve cells; two biological replicates; scale bar, 10 μ m; two-sided/unpaired t-test; n.s.=not significant; s=significant; n=number of cells.

Figure 2: Loss of *Prdm1* and *Nanog* affects PGCLC specification.

- a**, Analysis (qPCR) of mutant (*Prdm1*^{-/-}) and control (*Prdm1*^{+/+}) unsorted cells following *Nanog* expression (+Dox). $\Delta\Delta$ Ct +/- s.d (n=2 technical replicates each from 2 biological replicates); two-sided/unpaired t-test: **p<0.01; *p<0.05.
- b**, *Nanog* frameshift mutant alleles.
- c**, Western blot for NANOG and α -TUBULIN (α -TUB) as depicted. +/-Dox for 2 days; gel source data in Supplementary Fig.1.
- d**, Experimental design for **e-f**.

e, PGCLC induction in *Nanog*-KO cells, and rescue by *Nanog* (+Dox). Merged brightfield/GFP at D4; GFP+ve cells (%) after FACS; scale bar, 200 μ m.

f, Analysis (qPCR) of ESCs and D4 PGCLC aggregates shown in (**e**). $\Delta\Delta$ Ct +/- s.d. (n=2 technical replicates each from 2 biological replicates); two-sided/unpaired t-test: **p<0.01.

Figure 3: Competence for PGCLCs versus reversion to ESCs.

a, Experimental design for **b**, **c**.

b, Brightfield/GFP depicting D1/D2 EpiLCs in 2i/LIF+*Nanog* (+Dox); note D1 EpiLCs revert to ESCs, and attempted PGCLC induction in D1 EpiLCs also results in ESC reversion (see **c**). Scale bar, 200 μ m.

c, qPCR analysis; $\Delta\Delta$ Ct +/- s.d. (n=2 technical replicates each from 2 biological replicates); ESCs as reference for p-values (two-sided/unpaired t-test): **p<0.01; *p<0.05.

d, Western blot for NANOG, SOX2 and α -TUBULIN (α -TUB) with ESCs as depicted; +/-Dex/Dox for 2 days. Experimental design in Extended Data Fig. 7b; gel source data in Supplementary Fig. 1.

e, Analysis (qPCR) after *Sox2*-KO (+Dex) and *Nanog* induction (+Dox); $\Delta\Delta$ Ct +/- s.d. (n=2 technical replicates each from 2 biological replicates); parental ESCs as reference for p-values (two-sided/unpaired t-test): **p<0.01; *p<0.05. Experimental design in Extended Data Fig. 7e.

f, PGCLC induction with Dox-inducible transgenes (*Nanog*, *Sox2* or *Nanog/Sox2*); D4 brightfield/GOF-GFP+ve cells (%) after FACS; scale bar, 200 μ m.

Figure 4: Context-dependent NANOG binding in ESCs/EpiLCs.

a, qPCR analysis; induction of *Prdm1/Prdm14/Tfap2c* by *Nanog* (+Dox) in EpiLCs; $\Delta\Delta$ Ct +/- s.d. (n=3 technical replicates each from 2 biological replicates).

b, Genome-wide NANOG binding in D2 EpiLCs 3h after *Nanog* (+Dox). ‘Distal’ intergenic’ peaks: +/-50kb of coding gene, and those further away designated as ‘intergenic’.

c, NANOG ChIP-seq in ESCs and D1/D2 EpiLCs, with specific or shared high-confidence peaks; n=2 biological replicates.

d, ChIP-seq tracks^{9,30} at *Prdm1* and *Prdm14* loci, with putative enhancers (boxed) analysed in (**e-g**). RPM = Reads per Million.

e, Analysis of *Prdm1* enhancer-luciferase reporter in ESCs, EpiLCs, and after PGCLC induction (+Dox, EpiLC aggregations, unsorted). Mean luciferase activity normalised to protein quantity (luc/pro) +/- s.d. (n=3 technical replicates). Reference for p-value (two-sided/unpaired t-test): EpiLC aggregations -Dox; **p<0.01; *p<0.05. Controls and replicates in Extended Data Fig. 10c, e.

f, SOX2 ChIP-qPCR in ESCs and 6h after PGCLC induction +/-Dox (+/-Sox2) (unsorted EpiLC aggregations). Mean of fold enrichment over negative region +/- s.e. (n=2 technical replicates each from 2 biological replicates); reference for p-values (two-sided/unpaired t-test): IgG; *p<0.05.

g, Analysis of *Prdm14* enhancer-luciferase reporter in ESCs, EpiLCs and after PGCLC induction (+Dox, EpiLC aggregations, unsorted). Mean luciferase activity normalised to protein quantity (luc/pro) +/- s.d. (n=3 technical replicates); reference for p-values (two-sided/unpaired t-test): EpiLC aggregations -Dox 24h; **p<0.01. Colour code as in (**e**); controls and replicates in Extended Data Fig. 10c, e.

Methods

Animals

Timed natural matings were used for all experiments, where noon of the next day after the vaginal plugs of mated females were identified was scored as E0.5. Animal studies were authorized by a UK Home Office Project License and carried out in a Home Office-designated facility.

Mouse embryonic stem cells

Δ PE-Oct4-GFP (GOF-GFP)^{31,32}, *Blimp1*-GFP and *Prdm1*^{-/-} ESC lines were established previously^{14,19,22,23}. Inducible Sox2 knockout (2CG2) ESC line was a gift by Dr. Hitoshi Niwa²⁷. All ESC lines were maintained in naïve 'ground state'³³ condition; i.e. in N2B27 medium (R&D) with 2i (PD0325901, 1 μ M; CHIR99021, 3 μ M; Stemgent), LIF and 1% KnockOut Serum Replacement (KSR; Life Technologies) on Fibronectin-coated dishes (16.7 μ g/ml; Millipore). Medium was changed daily. ESC colonies were passaged by dissociating with TrypLE (Life Technologies).

Establishment of PiggyBac based Tet-on expression system during PGCLCs induction

Oct4, *Sox2*, *Nanog*, *Prdm1*, *Prdm14* and *Brachyury* cDNAs were cloned from mouse cDNA pool.

cDNAs were inserted into PiggyBac based doxycycline (Dox) inducible vectors (a gift of Dr. Hitoshi Niwa). These vectors were transfected using Lipofectamine 2000 (Life Technologies) into ESCs together with a pPyCAG-PBase vector and a pPBCAG-rtTAIRESNeo^r vector, which harbours a neomycin resistance gene. After 1 week of neomycin (80 µg/ml; Life Technologies) selection, pooled or single clones were used for experiments. To induce transgene expression, various concentrations of Dox (Sigma-Aldrich) were added to the media.

Induction of EpiLCs and PGCLCs

EpiLCs and PGCLCs were induced as described previously⁵. Transgenes were induced by addition of Dox at day0 of PGCLC induction. 100 ng/ml Dox was used in experiments shown in Fig. 3f, 4e, g, Extended Data Fig. 3b, c, 7g-i, 8a-c. 200 ng/ml Dox was used in Fig. 4b-d, f. 700 ng/ml of Dox was used in all other experiments. PGCLCs were induced as described in the manuscript. For inhibition of the BMP-SMAD pathway, Noggin (200 ng/ml; R&D) was added in the media at day0 of PGCLC induction. For inhibition of Wnt signalling, XAV939 (1 µM; Sigma-Aldrich) was added to the media.

Reversion of epiblast-like cells into ES-like cells

D1 or D2 EpiLCs were transferred into GMEM 15%KSR 2i LIF with or without Dox in monolayer culture. In addition, D1 or D2 EpiLCs were aggregated in low-cell-binding U-bottom shaped 96-well plates (Thermo Scientific) (1000-2000 cells per well) in PGCLC induction media (GMEM with L-glutamine (Life Technologies), 15% KSR (Life Technologies), 1x MEM NEAA (Life Technologies), 1x Sodium Pyruvate (Life Technologies), 1x 2-mercaptoethanol (Life Technologies), 1x Penicillin/Streptomycin (Life Technologies)) and Dox, The medium was replaced daily. After 3 days, the GFP reporter signal was analysed with a fluorescence microscope and *via* Fluorescence-Activated Cell Sorting (FACS) analysis. RNA was collected from pooled cells for qRT-PCR.

Embryonic germ cell-like cell (EGCLCs) derivation

D4 aggregates were dissociated with TrypLE and plated on mouse embryonic feeder cells (MEFs) with PGC selection medium (DMEM with L-glutamine (Life Technologies), 15% Fetal Bovine

Serum (FBS, Sigma-Aldrich)), LIF, 15 ng/ml bFGF, 30 ng/ml SCF (R&D) and 2 μ M All trans-retinoic acid (Sigma-Aldrich). Retinoic acid promotes germ cell self-renewal while promoting differentiation of ESCs^{20,21}. The media was replaced daily. After 5 days, proliferating GFP+ve cells were dissociated with TrypLE and plated on Fibronectin-coated dishes with ESC medium (N2B27 with 2i LIF).

Fluorescence-Activated Cell Sorting (FACS)

PGCLCs were dissociated with TrypLE, washed with DMEM containing 10% FBS and re-suspended with 1xPBS containing 0.1% BSA. Large clumps of cells were removed using a cell strainer (BD Biosciences). The cells were analysed and sorted on flow cytometers (FACS Calibur, BD Biosciences; MoFlo high speed cell sorter, Beckman Coulter; S3 cell sorter, Biorad). FACS plots show FL1; green on x-axis and SSC; side scatter on y-axis.

RT-qPCR

Total RNAs from ESCs, EpiLCs and FACS-sorted cells were extracted using the RNeasy Mini Kit (Qiagen) or Picopure RNA Isolation Kit (Life Technologies). The total RNAs were reverse transcribed by the Quantitect Reverse Transcription Kit (QIAGEN). The first-strand cDNAs were used for RT-qPCR analysis with SYBR Green PCR reagent (Sigma-Aldrich). The primer sequences used for the qRT-PCR are listed in Supplementary Table 1. Student's t-test was used to test for significance.

Microarray

ESCs and D4 PGCLC were dissociated and sorted with a MoFlo high-speed cell sorter (Beckman Coulter). Total RNAs were extracted using the RNeasy Mini Kit (QIAGEN). Complementary RNA (cRNA) generation, quality control, hybridization and data analysis were performed by Cambridge Genomic Services at the University of Cambridge. Raw intensity values from Illumina MouseWG-6 v2.0 expression beadchip microarrays were pre-processed with the Bioconductor *lumi* and *preprocessCore* packages (www.bioconductor.org): Probes that were not detected in at least one sample were removed, Variance Stabilization Transformation (VST) was applied, and samples

were quantile-normalized. Differential expression was evaluated with the Bioconductor *limma* package.

Comparison with published microarray data (Extended Data Fig. 3j): Our data set has been assayed on an Illumina MouseWG-6 v2.0 expression beadchip, the data set from Hayashi et al. (2011)⁵ on the Affymetrix Mouse Genome 430 2.0 Array platform. We therefore quantile-normalized the data sets to ensure that the data sets span comparable ranges of expression values. Principal component analysis (PCA) was performed on the center-scaled expression values, where systematic differences between platforms are mainly captured by the first principal component.

Immunofluorescence stainings

D3, D4 and D6 aggregates were fixed with 2% or 4% paraformaldehyde for 20 minutes at RT or for 2h at 4°C. Fixed aggregates, were washed several times in PBS and transferred into 10% sucrose/PBS (2h), 20% sucrose/PBS (2h) and finally into OCT embedding matrix (over night; CellPath). Next day, cell aggregates were embedded in OCT in tissue molds and stored at -80°C. A Leica Cryostat CM3050S was used to cut the OCT blocks in 6-8µm thick sections, which were collected on SuperFrost Plus slides (VWR).

For immunofluorescence staining, the slides were washed with PBS, permeabilised with PBS/0.1-1% Triton X-100 and then incubated with primary antibodies in permeabilisation buffer including 5% donkey serum (Sigma-Aldrich) over night at 4°C. Next day, slides were washed with PBS and incubated with secondary antibodies in permeabilisation buffer for 2h at RT, washed with PBS, incubated with DAPI in PBS for 15-30 minutes, and mounted using Vectashield Mounting Medium (VECTOR Labs). Images were acquired using a Leica SP5 or SP8 confocal microscope. For 5-hmC stainings, it was required to perform an additional antigen retrieval step before incubation with primary antibodies: slides with sections were transferred into TE buffer, pH8, at ~95°C and microwaved at very low power for 45 minutes.

The following primary antibodies were used: mouse anti-OCT4 (1:100, BD Biosciences, O50808), rat anti-BLIMP1 (1:50, eBioscience, clone 6D3, 14-5963), rabbit anti-AP2γ (1:250, SantaCruz, sc-8977), rabbit anti-PRDM14 (1:250, a kind gift of Prof. Danny Reinberg), rabbit anti-DAZL (1:500,

Abcam, ab34139), mouse anti-H3K9me2 (1:250, Abcam, ab1220 and 1:500, Millipore, 07-441), rabbit anti-H3K27me3 (1:500, Millipore, 07-449), rabbit anti-TET1 (1:500, Millipore, 09-872), rabbit anti-5hmC (1:500, Active Motif, 39791), goat anti-KLF4 (1:100, R&D, AF3158), rabbit anti-H3S10ph (1:500, Millipore, 06-5770), mouse anti- γ H2A.X (1:250, Millipore, 05-636), rat anti-GFP (1:500, Nakalai Tesque, GF090R) and Alexa Fluor488 and 568 secondary antibodies (1:500, Life Technologies) were used.

Quantification of immunofluorescence data

All quantifications were performed using Fiji³⁴. The DAPI, H3S10ph and γ H2A.X channels were processed by applying a Gaussian Blur (H3S10ph staining: DAPI/H3S10ph - σ 0.5/1.1; DAPI/ γ H2A.X: σ 1.0/1.5) to reduce noise. The images were then binarized using the Otsu thresholding algorithm and holes were filled before the total signal area was measured. In D6 *Prdm1*^{-/-} +Dox aggregates, many cells underwent cell death. Therefore, nuclei with bright discrete spots of DAPI signal, which indicates chromatin condensation, were excluded from the analysis. The diameter of ~10 cells was measured and used to calculate the average area of one cell in order to estimate the number of cells in the field of view (DAPI+ve area/area of one cell).

For all other quantifications on a single cell level, we developed 'Object Scan', which is an object mapping and analysis plugin for Fiji that combines advanced functions with a user-friendly interface. Images are processed with a choice of feature enhancement algorithms, objects are identified by patch sampling to detect intensity edges based on the local energy gradient, and the generated two-dimensional masks are clustered in three dimensions to define the final object map for analysis. We used Object Scan to carry out DoG processing and contained signal analysis using the DAPI channel for object mapping, watershed segmentation, a scan radius of one and the following channel specific settings: edge gradient = 10, estimated object radius = 9 μ m. The results were scale normalised ($(X-X_{min})/(X_{max}-X_{min})$) to the range 0 to 1 for comparison. Student's t-test was used to test for significance. The Object Scan plugin is available from this link: <http://www.gurdon.cam.ac.uk/stafflinks/downloadpublic/imaging-plugins>.

Chromatin immunoprecipitation (ChIP)

Low cell number ChIP-qPCR was performed as previously described³⁵. 3×10^5 cells per ChIP were fixed in 1% formaldehyde (room temperature, 10 min), quenched with 1 vol. of 250 mM glycine (room temperature, 5 min), and rinsed with chilled TBSE buffer (20 mM Tris-HCl, 150 mM NaCl, 1 mM EDTA) twice before storage at -80°C . After thawing the cells on ice, fixed cells were lysed with 100 μl 1% SDS Lysis Buffer (50mM Tris-HCl pH8, 10mM EDTA, 1% SDS, Roche protease inhibitor cocktail; on ice, 5 min) and then centrifuged (2,000 rpm, 10 min). Pellet was resuspended in 100 μl of Dilution buffer (16.7mM Tris-HCl, pH8, 167mM NaCl, 1.2mM EDTA, 1.1% Triton X-100, 0.01% SDS, Roche protease inhibitor cocktail). Samples were sonicated 9 times (30 s pulses with 30 s break interval) using the Bioruptor water bath sonicator (Diagenode). Chromatin extracts were then precleared with Dynal Magnetic Beads (Invitrogen) (4°C , 1 hr) followed by centrifugation (2,000 rpm, 30 min). Supernatant (precleared chromatin) was immunoprecipitated overnight with Dynal Magnetic Beads coupled with anti-Nanog antibody (1 μg per ChIP, Cosmo Bio Co., RCAB0001P) or normal rabbit serum (1 μg per ChIP). On the next day, beads were washed (nutate in wash buffer for 5 min at 4°C) in low salt buffer (0.1% SDS, 1% TritonX-100, 2 mM EDTA, 20 mM Tris-HCl, pH 8.0, 150 mM NaCl), high salt buffer (0.1% SDS, 1% TritonX-100, 2 mM EDTA, 20 mM Tris-HCl, pH 8.0, 300 mM NaCl) and LiCl buffer (0.25M LiCl, 1% NP400, 1% Na deoxycholate, 1 mM EDTA, 10 mM Tris-HCl, pH 8.0), for a total of three washes. Following an additional wash in TE, elution was performed in a PCR machine (68°C , 10 min). After digesting and reverse crosslinking (with Proteinase K at 42°C for 2 hr and 68°C for 6 hr) DNA was purified (phenol-chloroform extraction) and used for qPCR analysis. For the negative control region, we used the *Snai3* locus as described previously³⁶. Student's t-test was used to test for significance.

The same protocol was used for the SOX2 ChIP with some deviations. D2 EpiLCs were aggregated in low binding plates for 6h in the presence of 200 ng/ml of Doxycycline before collection. 5×10^6 ESCs and EpiLCs, respectively, were fixed and processed as described above. Samples were sonicated 20 times (30 s pulses with 30 s break interval) using a Bioruptor water bath sonicator (Diagenode). Samples were divided for immunoprecipitations with SOX2 antibody (10 μg per ChIP, Santa Cruz, sc-17320 X) or normal rabbit IgG (10 μg per ChIP, Santa Cruz, sc-2027 X) as a negative control. Beads were washed with low salt buffer, and 2x with high salt buffer for 10 minutes each. The beads were rinsed in TE, resuspended in Proteinase K digestion buffer

(20mM HEPES, 1mM EDTA, 0.5% SDS) with 2µl of 10mg/ml Proteinase K and incubated for 15 min at 50C. In parallel, 2µl of 10mg/ml Proteinase K was added to the saved input samples. 3µl 5M NaCl was added to the supernatants and the input samples. To reverse the crosslinks, samples were incubated at 42C for 2h and 68C over night. Next day, the DNA was purified using Agencourt Ampure XP beads (Beckman Coulter) according to manufacturer's instructions. The purified DNA was used for qPCR analysis. For the negative control region, we used the *Snai3* locus. Student's t-test was used to test for significance. The primer sequences used for RT-qPCRs are listed in Supplementary Table 1.

NANOG ChIP-seq

The NANOG ChIP for subsequent sequencing was performed as described above with some deviations. D1 or D2 EpiLCs were aggregated in low binding plates for 3h in the presence of 200 ng/ml of doxycycline. ESCs and EpiLCs were fixed and processed as described above. 3×10^6 fixed cells were lysed with 1 ml 1% SDS Lysis Buffer and then centrifuged (2,000 rpm, 15 min). Nuclear fraction was resuspended in 0.9 ml of dilution buffer. Samples were sonicated 10 times (30 s pulses with 30 s break interval) using a Bioruptor water bath sonicator (Diagenode). Immunoprecipitations were performed with anti-NANOG antibody (2µg per ChIP, Cosmo Bio Co., RCAB0001P). After elution samples were digested with Proteinase K and reverse crosslinked for 6 h at 68°C. 12 ng of purified DNA was used for library preparation using Ovation Ultralow DR Multiplex System (Nugen). Once prepared, library was size selected and sequenced using HiSeq2000 with single-end 50 nt read length.

ChIP-Seq analysis

ChIP-seq reads were aligned with the *bwa* aligner (bio-bwa.sourceforge.net) to the mouse reference genome (GRCm38/mm10). Peaks were called with *MACS* (version 2.1.0 <https://github.com/taoliu/MACS>) and visualised using the Integrative Genomics Viewer (<https://www.broadinstitute.org/igv/>). Peak regions from two biological replicates were intersected using *bedops* (bedops.readthedocs.org). Overlapping peak regions with peak summits within < 50 nt distance in both replicates were retained. Peak regions from the three cell types were merged.

Differences in ChIP-seq read intensities on peak regions were evaluated by using *diffReps* (code.google.com/p/diffreps) and MACS (*macs2 bdgdiff*). High-confidence sets of differentially bound regions that were detected by both methods were selected for further analysis by applying the following thresholds for *diffReps*: $p\text{Value} < 0.001$ and $\text{abs}(\log_2\text{FC}) > 1$. Previously published H3K27ac ChIP-seq data sets^{9,30} were aligned to the mouse reference genome in a similar manner as above, and H3K27ac enrichment ($\log(\text{ChIP}/\text{input})$) values were determined on NANOG peak regions.

De novo motif analysis

High-confidence MACS peaks, for which the distance of the peak summits in both replicates was <50 nt, were selected. *De novo* motifs were determined with HOMER (<http://homer.salk.edu/homer>) in the 2,000 top-enriched peaks in ESCs, D1 and D2 EpiLC for both repeat-masked and repeat-unmasked regions within +/- 50 nt of the peak summit.

Luciferase assay

Genomic regions containing putative enhancers of *Prdm1* and *Prdm14*, as well as a negative control region depleted of enhancer signatures, were amplified from mouse E14 ESC genomic DNA. These regions were cloned into a PiggyBAC-based firefly luciferase reporter plasmid upstream of a minimal TK promoter. Stable luciferase reporter GOF-GFP ESC lines, which can overexpress *Nanog*, *Nanog/Sox2* or *Brachyury* upon Dox addition, were established. Cell pellets were collected from ESCs cultured in N2B27 2i LIF, D2 EpiLCs and EpiLCs after PGCLC induction +/- Dox at 12/24 hours. Luciferase assays were performed with the ONE-Glo™ Luciferase Assay System (Promega). Protein concentration in each lysate was quantified by Pierce 660 nm Protein Assay (Thermo Scientific). Relative luciferase activities were obtained by dividing luciferase activity by protein concentration in each sample.

Blastocyst injections

ESC clones carrying both the *Nanog* transgene and a CAG monomeric Kusabira-orange (mKO) fluorescence reporter were selected by neomycin (Sigma-Aldrich) and zeocine (Life Technologies).

D4 PGCLCs were induced from D2 EpiLCs with *Nanog* and used for derivation of EGCLC. For ESC or D4 PGCLC injections, GOF-GFP ESCs were co-transfected with a vector, which enabled inducible expression of *Nanog* and constitutive expression of Venus, a variant of EGFP. For D4 PGCLC, after induction of PGCLCs with *Nanog*, cells were stained with PE conjugated-CD61 antibody (1:10, Biolegend, 104308) and Alexa660 conjugated-SSEA-1 antibody (2.5 μ l/ 10^5 cells, eBioscience, clone eBioMC-480, 50-8813) according to the manufacturer's instructions. Double positive PGCLC cells were collected by using a S3 cell sorter (Biorad). Embryos for chimera experiments were obtained from CBA/C57BL/6 F1 crossed with C57BL/6 mice. Blind tests or randomization methods were not used. The sex of embryos was not determined. Manipulations of embryos were performed as described previously³⁷. Briefly, five cells were injected into a morula, which were subsequently cultured in KSOM (Millipore). At the following day, the embryos were transferred into the uteri of pseudopregnant mice. All embryos were analysed one week after embryo transfer, which corresponded to embryonic day 9.5.

Generation of *Nanog* knockout ESCs

The CRISPR/Cas9 system was used to generate *Nanog* knock-out ESCs. gRNAs targeting exon1 of the *Nanog* gene were cloned into pX330³⁸ (Addgene). 1 μ g of this plasmid was transfected with a pPyCAG-monomeric Kusabira Orange-IRES-Pac plasmid. Transfected cells were selected by puromycin (1 μ g/ml) for 2 days. Clonal *Nanog* KO ES lines were established and mutations of *Nanog* alleles were confirmed by QPCR, Western blotting and DNA sequencing. Subsequently, pPBhCMV*1-*Nanog*-pA plasmid was transfected into those lines with pPyCAG-PBase and pPBhCMV*1-rtTA-IRESNeo^r to generate *Nanog* KO ESC lines carrying a Dox-inducible *Nanog* transgene. Loss of *Nanog* affected the growth of ESCs. Thus, these cell lines were maintained in N2B27 2i LIF with a low dose of Dox (100 ng/ml). gRNA sequences are listed in Supplementary Table 1.

Western blots

5 x 10^4 cells were lysed in lysis buffer (50 mM Tris-HCl [pH 8.0], 1% SDS, 10 mM EDTA). Protein concentration was measured by Bicinchoninic Acid Kit (Sigma-Aldrich). The protein amount was

adjusted among samples, then 4x Laemmli buffer was added. Samples were boiled at 95°C for 5 min. Proteins were separated on 10% acrylamide gels, blotted on Immobilon-P transfer membrane (Millipore). The membrane was blocked with 5% skimmed milk and incubated with primary antibodies: anti-NANOG (1:500, mouse IgG, eBioscience, clone eBioMLC-51, 14-5761), anti-SOX2 (1:500, rabbit igG, Cell Signaling, 2748), anti- α -TUBULIN (1:1000, mouse IgG, Sigma-Aldrich, clone DM1A, T9026). Primary antibodies were detected on X-ray film with anti-rabbit or -mouse IgG conjugated with Horseradish peroxidase (Dako) followed by detection using Western Detection System (GE Healthcare). For gel source data, see Supplementary Figure 1.

Generation of Sox2 conditional knockout ESCs with Dox-inducible *Nanog* transgene

pPBhCMV*1-*Nanog*-pA, pPBCAG-rtTA-IRESNeo^r and pPyCAG-PBase were transfected into the Sox2 conditional knockout ESC line (2CG2)²⁷. After one week of neomycin selection (80 μ g/ml), pooled cells were used for the subsequent experiments. Dexamethasone-inducible Sox2 KO and Dox-inducible *Nanog* expression were confirmed by qPCR and Western blotting.

Extended Data Figure Legends

Extended Data Figure 1: GOF-GFP as a reporter for PGCLCs; Dox-inducible transgene system.

- a**, Experimental design for the induction of PGCLCs *in vitro*⁵.
- b**, Representative brightfield/GFP images of male/female GOF-GFP ESCs, D2 EpiLCs, D2 and D4 cytokine-induced PGCLCs. Scale bar, 200 μ m.
- c**, FACS analysis for GFP with samples shown in **(b)**.
- d**, Simplified scheme of PiggyBac (PB 5'TR and PB 3'TR) based plasmids for transgene overexpression using the Tet-On system. The rtTA protein activates the minimal promoter (hCMV*-1) driving the expression of the cDNA of interest only in the presence of doxycycline (Dox).
- e**, Proof of principle experiment to test the Dox-inducible expression of a transgene during the sequential differentiation of PGCLCs from ESCs. GOF-GFP ESCs carrying PiggyBac based Dox-inducible *mCherry* expression plasmids were differentiated into D2 EpiLCs and then induced into

PGCLCs with cytokines in +/-Dox conditions. Representative brightfield, GFP and mCherry images are shown 12h after aggregation. Scale bar, 200 μ m.

f, Representative FACS analysis for GFP and mCherry of D2 cytokine-induced PGCLCs from male/female GOF-GFP ESCs carrying a Dox-inducible *mCherry* transgene. Most cells express mCherry after Dox addition.

Extended Data Figure 2: *Nanog* but not *Oct4* induces GFP+ve cells from competent EpiLCs.

a, qPCR analysis of transgenic *Nanog* expression 24h after Dox addition in male/female GOF-GFP ESCs. $\Delta\Delta$ Ct mean values +/- s.d. (n=2 technical replicates each from 2 biological replicates). Two-sided/unpaired t-test: **p<0.01. Related to Fig. 1a.

b, Representative brightfield/GFP images of male D2 PGCLCs induced from GOF-GFP D2 EpiLCs; +Dox for *Nanog* expression. Scale bar, 200 μ m. Related to Fig. 1a.

c, Representative FACS analysis of male D4 PGCLCs (shown in Fig. 1a) induced from GOF-GFP D2 EpiLCs; +Dox for *Nanog* expression.

d, Representative brightfield/GFP images of female D2 and D4 PGCLCs induced from GOF-GFP D2 EpiLCs; +Dox for *Nanog* expression. Scale bar, 200 μ m. Related to Fig. 1a.

e, FACS analysis for GFP with samples shown in (d). Related to Fig. 1a.

f, qPCR analysis of transgenic *Oct4* expression 24h after Dox addition in male ESCs. $\Delta\Delta$ Ct mean values +/- s.d. (n=2 technical replicates each from 2 biological replicates). Two-sided/unpaired t-test: **p<0.01.

g, Expression of *Oct4* (unlike *Nanog*) does not result in the induction of GFP+ve cells. PGCLC induction from female GOF-GFP EpiLCs; +Dox for *Oct4* or *Nanog* expression. Representative brightfield/GFP images at D4. Scale bar, 200 μ m.

h, FACS analysis for GFP with samples shown in (g).

Extended Data Figure 3: The transcriptomes of D4 *Nanog*- and cytokine-induced PGCLCs are highly similar.

a, 100-200 ng/ml of Dox in EpiLCs results in NANOG expression levels similar to ESCs as shown by Western blot analysis for NANOG and α -TUBULIN (α -TUB) with GOF-GFP ESCs and D2

EpiLCs 24h after PGCLC induction (EpiLC aggregations) with *Nanog* (+Dox). For gel source data, see Supplementary Fig. 1.

b, PGCLC induction with 100 or 700 ng/ml Dox (for *Nanog* expression) with Noggin from GOF-GFP EpiLCs. Representative brightfield/GFP images at D4. GFP+ve cells are induced in both conditions. Scale bar, 200 μ m.

c, Physiological (equivalent to ESCs) or higher levels of *Nanog* induce PGCLCs with comparable efficiency. FACS for GFP at D4 of PGCLC induction with 100 or 700 ng/ml Dox (for *Nanog* expression) with Noggin from GOF-GFP or *Blimp1*-GFP EpiLCs.

d, Alternative representation of qPCR data for *Nanog*, *Prdm1* and *Tfap2c* shown in Fig. 1c. The induction of these genes in +cytokine conditions appears less evident, when compared to +Dox conditions. The data was \log_2 -scaled, which allows a better comparison.

e, qPCR analysis of female GOF-GFP cells. GFP+ve cells were FACS-sorted. Note, the upregulation of PGC markers but not of the ESC marker *Klf4*. $\Delta\Delta$ Ct mean values \pm s.d. (n=3 biological replicates). Colour code is shown in (**d**). Related to Fig. 1c.

f, qPCR analysis of male *Blimp1*-GFP cells. GFP+ve cells were FACS-sorted. Note, the upregulation of PGC markers but not of the ESC marker *Klf4*. $\Delta\Delta$ Ct mean values \pm s.d. (n=3 biological replicates). Colour code is shown in (**d**). Related to Fig. 1c.

g, The transcriptomes of *Nanog*- and cytokine-induced PGCLCs are highly similar. Scatter plot showing the correlation of microarray data of ESCs, FACS-sorted D4 PGCLCs induced by cytokines or *Nanog* with Noggin. R indicates the Pearson correlation coefficient. n=2 biological replicates; related to Fig. 1d.

h, *Nanog*- and cytokine-induced PGCLCs cluster together as shown in unsupervised hierarchical clustering of microarray data described in (**g**). Related to Fig. 1d.

i, Heatmap showing the expression levels of selected genes from microarray data described in (**g**). Related to Fig. 1d.

j, *Nanog*-induced D4 PGCLCs are closely related to cytokine-induced D6 PGCLCs. PCA analysis with published microarray datasets⁵ (cross-platform comparison; see Methods for details). Note, that the separation of ESC samples is probably due to differences in genomic background and culture conditions.

Extended Data Figure 4: *Nanog*-induced PGCLCs show hallmarks of PGC development.

a-c, IF analysis of PGC markers in GFP+ve cells induced by *Nanog* from male (**a**) and female (**b**) GOF-GFP and male *Blimp1*-GFP (**c**) EpiLCs shows expression of BLIMP1, PRDM14, and AP2 γ , TET1, enrichment of H3K27me3 and 5hmC and a decrease of H3K9me2 intensity; DAZL is detected in some cells on D6. Arrowheads and dashed lines highlight single or cluster of GFP+ve cells. n=2 biological replicates; scale bar, 10 μ m. Quantification in (**c**) was scale normalised. Two-sided/unpaired t-test: n.s.=not significant; s=significant; n=number of cells analysed. Related to Fig. 1e.

Extended Data Figure 5: Functional analysis of *Nanog*-induced PGCLCs.

a, Experimental design (for **b**, **c**) for the derivation of EGC-like cells (EGCLCs). PGCLCs were induced with cytokines or by *Nanog* (+Dox) from male or female GOF-GFP EpiLCs carrying a constitutively active Kusabira-Orange reporter. On D4, aggregations were dissociated and cultured on MEF in PGC selection medium (LIF, SCF, bFGF, retinoic acid) for 5 days. After the selection, selected colonies were dissociated and transferred into ESC medium (2i LIF).

b, Experiment was performed as shown in (**a**). Left panel shows representative images of proliferating GFP+ve cells after 3 days of PGC selection. Right panel shows established EGCLCs after 3 passages in 2i LIF.

c, EGCLCs derived from D4 PGCLCs by *Nanog* expression were injected into blastocysts resulting in high contribution to chimeras at E9.5 as shown by Kusabira-Orange expression.

d, Experimental design (for **e-g**) for generating chimeras. PGCLCs were induced from a GOF-GFP ESC line expressing a fluorescent VENUS reporter constitutively and *Nanog* upon Dox addition (TVN2 cell line). On D4, aggregations were dissociated and SSEA1+ve and CD61+ve cells were sorted by FACS, injected into morulae and analysed on E9.5.

e, Representative brightfield, GFP/VENUS images of GOF-GFP or TVN2 cells during PGCLC induction by cytokines or *Nanog* (+Dox). Scale bars, 100 μ m.

f, FACS profile for SSEA1+ve and CD61+ve PGCLCs on D4 induced as described and shown in (**d**, **e**).

e, ESCs but not PGCLCs contribute efficiently to chimeras. ESCs or FACS-sorted *Nanog*-induced SSEA1+ve/CD61+ve PGCLCs were injected into morulae and representative brightfield/VENUS images from chimeras at E9.5 are shown.

Extended Data Figure 6: *Prdm1*^{-/-} abrogates PGCLC induction by *Nanog*; *Nanog* and the Wnt pathway act independently.

a, PGCLC induction with cytokines or *Nanog* (+Dox) from *Prdm1*^{-/-} ESCs (*Prdm1*^{-/-}; *Nanog*). Representative brightfield images of D4 and D6 aggregations. Scale bar, 200 μm. Related to Fig. 2a.

b, Loss of *Prdm1* abrogates PGCLCs induced by NANOG as shown by qPCR analysis of mutant (*Prdm1*^{-/-}; *Nanog*) compared with control (*Prdm1*^{+/+}; *Nanog*) cells with *Nanog* (+Dox) or cytokines (+cyto). Unsorted samples were used for analysis. Note that the data shown in Fig. 2a was combined with additional qPCR data on cells at D6 of PGCLC induction. $\Delta\Delta C_t$ mean values +/- s.d. (n=2 technical replicates each from 2 biological replicates); two-sided/unpaired t-test: **p<0.01; *p<0.05. Related to Fig. 2a.

c, *Nanog* does not affect cell proliferation rate of *Prdm1*^{-/-}; *Nanog* cells. IF staining for the mitotic marker H3S10ph in *Prdm1*^{-/-}; *Nanog* cells at D6 of PGCLC induction; +Dox for *Nanog* expression. Scale bar, 10μm; two-sided/unpaired t-test; n.s.=not significant; n=estimated number of cells (see Methods for details). Related to Fig. 2a.

d, Induced expression of *Nanog* results in an increased number of cell death of *Prdm1*^{-/-}; *Nanog* cells. IF stainings of the DNA double strand break marker γH2AX in *Prdm1*^{-/-}; *Nanog* cells at D6 of PGCLC induction; +Dox for *Nanog* expression. Scale bar, 10μm; two-sided/unpaired t-test; s=significant; n=estimated number of cells (see Methods for details). Related to Fig. 2a.

e, Experimental design (for f-i) to test the interdependence of *Nanog* and the Wnt pathway for PGCLC induction. *Blimp1*-GFP ESCs were sequentially differentiated into PGCLCs +/- tankyrase inhibitor XAV939, which causes the degradation of β-catenin²⁵; +Dox for *Nanog* expression.

f, XAV939 does not affect the morphology and proliferation of D2 EpiLCs. Representative brightfield/GFP images of D2 EpiLCs induced from GOF-GFP ESCs with 1μM XAV939. Scale bar, 200μm.

g, qPCR of D2 EpiLCs treated with XAV939 as shown in **(a, b)**. The expression of *Nanog* and of the EpiLC markers *Dnmt3a* and *Dnmt3b* are not affected by XAV939. *Brachyury*, the downstream target of WNT, is most efficiently repressed with 1 μ M XAV939. $\Delta\Delta$ Ct mean values \pm s.d. (n=2 technical replicates each from 2 biological replicates); two-sided/unpaired t-test: **p<0.01; *p<0.05.

h, The efficiency of PGCLC induction by cytokines but not by *Nanog* (+Dox) is markedly reduced upon XAV939 addition. PGCLCs were induced from 1 μ M XAV939-treated D2 EpiLCs. Representative FACS analysis for GFP with cells at D4 of PGCLC induction.

i, XAV939 does not affect the induction of PGC marker expression in *Nanog*-induced PGCLCs. Gene expression analysis by qPCR with FACS-sorted *Nanog*-induced D4 PGCLCs \pm 1 μ M XAV939. Mean $\Delta\Delta$ Ct values \pm s.d. (n=2 technical replicates each from 2 biological replicates). Two-sided/unpaired t-test: **p<0.01; *p<0.05; n.s.=not significant.

Extended Data Figure 7: Sox2 inhibits PGCLC induction by *Nanog*.

a, *Prdm1* and *Tfap2c* are upregulated and *Prdm14* is downregulated in Sox2-KO ESCs from published microarray data²⁶. **p<0.01; *p<0.05.

b, Experimental design for the Western blot shown in Fig. 3d. Conditional Sox2-KO ESCs carrying transgenes for Dox-inducible *Nanog* expression were treated with Dex to induce a Sox2-KO and/or Dox for *Nanog* expression for 2 days.

c, Experimental design for the qPCR analysis shown in **(d)**. Sox2-KO ESCs: Conditional Sox2-KO ESCs carrying transgenes for Dox-inducible *Nanog* expression were treated \pm Dex for 2 days; Sox2-KO D1 EpiLCs: ESCs were cultured in 2i LIF medium with Dex for one day and in bFGF/ActivinA medium with Dex for one more day; Sox2-KO D2 EpiLCs: ESCs were transferred into bFGF/ActivinA medium containing Dex for two days.

d, Loss of *Sox2* results in upregulation of *Prdm1* and *Tfap2c* and downregulation of *Prdm14* in ESCs, D1 and D2 EpiLCs; qPCR analysis following Sox2-KO (+Dex). $\Delta\Delta$ Ct mean values \pm s.d. (n=2 technical replicates each from 2 biological replicates); two-sided/unpaired t-test: **p<0.01; *p<0.05. Experimental design is shown in **(c)**. Related to Fig. 3e.

e, Experimental design for the qPCR analysis shown in Fig. 3e. Sox2-KO ESCs, D1 or D2 EpiLCs were generated as described in **(c)**, and subsequently induced into PGCLCs \pm *Nanog* (\pm Dox).

f, Western blot for NANOG, SOX2 and α -TUBULIN (α -TUB) in GOF-GFP ESCs carrying Dox-inducible transgenes for *Nanog*, *Sox2* or *Nanog/Sox2* (+Dox for 24h). Related to Fig. 3f. For gel source data, see Supplementary Fig. 1.

g, Time-course qPCR analysis showing *Nanog* and *Sox2* expression kinetics during PGCLC induction. PGCLCs were induced from GOF-GFP EpiLCs; +100 or 700 ng/ml Dox for *Nanog/Sox2* expression. Related to Fig. 3f.

h, Time-course Western blot for NANOG, SOX2 and α -TUBULIN (α -TUB) showing *Nanog* and *Sox2* protein kinetics during PGCLC induction. PGCLCs were induced from GOF-GFP EpiLCs; +100 or 700 ng/ml Dox for *Nanog/Sox2* expression. Related to Fig. 3f.

i, FACS analysis for GFP at D4 of PGCLC induction from GOF-GFP or *Blimp1*-GFP EpiLCs; +Dox for *Nanog*, *Sox2* or *Nanog/Sox2* expression. Related to Fig. 3f. For gel source data, see Supplementary Fig. 1.

Extended Data Figure 8: Sox2 positively affects cell proliferation rate of cytokine-induced PGCLCs.

a, *Sox2* increases the number of GFP+ve cells induced by BMP4 alone. Representative FACS analysis for GFP at D4 of PGCLC induction from *Blimp1*-GFP EpiLCs; +Dox for *Sox2* expression.

b, *Sox2* does not affect the upregulation of PGC markers in cytokine-induced PGCLCs. qPCR analysis of FACS-sorted GFP+ve cells induced by BMP4 and/or *Sox2* (+Dox). $\Delta\Delta$ Ct mean values +/- s.d. (n=2 technical replicates each from 2 biological replicates). Reference sample for p-value calculations: ESCs; two-sided/unpaired t-test: **p<0.01; *p<0.05.

c, Time-course FACS analysis of GFP+ve cells after PGCLC induction with BMP4 and +/- *Nanog* or *Sox2* (+/- Dox). The number of GFP+ve cells at D2 of PGCLC induction with or without *Sox2* expression is comparable, but increased with *Nanog*. After D2, PGCLCs induced by BMP4 with *Sox2* or *Nanog* increase their proliferation rate.

Extended Data Figure 9: Nanog shows a cell-type specific binding pattern and induces Prdm1/Prdm14/Tfap2c.

a, Time-course qPCR for *Prdm1*, *Prdm14* and *Tfap2c* between 1-48h after PGCLC induction with cytokines from GOF-GFP EpiLCs. $\Delta\Delta\text{Ct}$ mean values \pm s.d. (n=3 technical replicates). Related to Fig. 4a.

b, *Prdm1* alone can induce the expression of *Tfap2c*. GOF-GFP EpiLCs with combinations of Dox-inducible transgenes encoding *Prdm1*, *Prdm14* and/or *Nanog* \pm Dox for 6h were analysed by qPCR. The expression of *Prdm1*, *Prdm14* and/or *Nanog* is upregulated in the corresponding EpiLCs upon Dox addition. $\Delta\Delta\text{Ct}$ mean values \pm s.d. (n=2 technical replicates each from 2 biological replicates); two-sided/unpaired t-test: **p<0.01; *p<0.05.

c, To acquire sufficient numbers of cells for ChIP-seq studies, GOF-GFP D1 or D2 EpiLCs ($\sim 1 \times 10^6$ cells per 6 cm plate) with Dox-inducible *Nanog* transgenes were aggregated in low binding plates +Dox to induce PGCLCs. qPCR analysis of D1 and D2 EpiLCs after 3h with 100 or 200 ng/ml Dox is shown. The addition of 200 ng/ml of Dox results in *Nanog* expression levels comparable to ESCs after 3h. $\Delta\Delta\text{Ct}$ mean values \pm s.d. (n=2 technical replicates each from 2 biological replicates); two-sided/unpaired t-test: **p<0.01; n.s.=not significant.

d, NANOG ChIP-seq analysis shows genomic distribution of NANOG in GOF-GFP ESCs and D1 EpiLCs +*Nanog* (+Dox) for 3h. 'Distal' refers to intergenic peaks, which are \pm 50kb of an annotated coding gene, while those further away are categorised as 'intergenic'. Related to Fig. 4b.

e, *De novo* motif analysis with NANOG ChIP-seq data. Shown are the 5 top matches of the *de novo* motifs to known motifs. The analysed cell types show enrichment for the NANOG and SOX motifs. ESCs show additional enrichment for pluripotency motifs, while EpiLCs show a different set of motif enrichment.

f, D2 EpiLC-specific (D2 EpiLCs +Dox 3h) NANOG-bound enhancers become more enriched for H3K27ac than ESC-specific NANOG-bound enhancers in cytokine-induced D2 PGCLCs as compared to ESCs. Contour plots showing differential binding of NANOG in D2 EpiLCs vs ESCs (x-axis) compared to the differential enrichment of H3K27ac in D2 PGCLCs³⁰ vs ESCs⁹ (y-axis).

g, NANOG binds enhancers that are enriched for H3K27ac in D1/D2 EpiLCs (D1/2 EpiLCs +Dox 3h). A subset of enhancers, however, becomes more enriched for H3K27ac in cytokine-induced D2 PGCLCs³⁰ as compared to D2 EpiLCs³⁰.

h, NANOG might contribute to the activation of enhancers associated with germline genes. Scatter plots show differential gene expression analysis between D6 PGCLCs⁵ and D2 EpiLCs⁵ (y-axis), and differential H3K27ac enrichment between D2 PGCLCs³⁰ and D2 EpiLCs³⁰ (x-axis) on NANOG binding sites. Top 40% of NANOG peaks were associated with the nearest gene in a 200kb window. Highlighted are candidate enhancers associated with germline genes. A selected set of genes associated with the germline and candidate enhancers, which become activated (H3K27ac-enriched) in PGCLCs, is indicated.

Extended Data Figure 10: *Nanog* induces PGC-like fate - a model

a, CHIP-seq data tracks^{9,30,39} at the *Prdm1* and *Prdm14* loci for NANOG in ESCs, D1 and D2 EpiLCs (EpiLCs were collected after 3h with 200 ng/ml Dox for *Nanog* expression). Boxed are putative enhancer elements. The *Prdm1* enhancer is enriched for H3K4me1 in D2 EpiLCs and gains H3K27ac in PGCLCs. The *Prdm14* enhancer shows enrichment for H3K4me1 in ESCs and EpiLCs and becomes enriched for H3K27ac in ESCs and PGCLCs but not in EpiLCs. Note that these enhancer marks follow the expression pattern of *Prdm1* or *Prdm14*, respectively. RPM = Reads per Million. Related to Fig. 4d.

b, CHIP-qPCR validation of NANOG CHIP-seq data with GOF-GFP D2 EpiLCs before and 3h after PGCLC induction by *Nanog* expression (+Dox). NANOG is enriched at putative enhancer regions, which are close to *Prdm1* and *Prdm14*. Error bars indicate s.d. (n=2 technical replicates each from 2 biological replicates).

c, ESC lines with luciferase reporter plasmids with a genomic region, which does not show any enhancer marks and NANOG binding, and indicated Dox-inducible transgenes served as a negative control. Luciferase activity, measured in ESCs, D2 EpiLCs and 24h after PGCLC induction (EpiLC aggregations), was normalised to protein quantity (luc/pro). Mean values +/- s.d. (n=3 technical replicates each from 2 biological replicates).

d, Biological replicate experiment for the luciferase assay with the *Prdm1* enhancer as shown and described in Fig. 4e. Luciferase activity, measured in ESCs, D2 EpiLCs and 24h after PGCLC induction, was normalised to protein quantity (luc/pro). Mean values +/- s.d. (n=3 technical

replicates); colour code is shown in (c); reference for p-values (two-sided/unpaired t-test): EpiLC aggregations -Dox; **p<0.01; *p<0.05.

e, Biological replicate experiment for the luciferase assay with the *Prdm14* enhancer as shown and described in Fig. 4g. Luciferase activity, measured in ESCs, D2 EpiLCs and 12/24h after PGCLC induction, was normalised to protein quantity (luc/pro). Mean values +/- s.d. (n=3 technical replicates); colour code is shown in (c); reference for p-values (two-sided/unpaired t-test): EpiLC aggregations -Dox 24h; **p<0.01; *p<0.05.

f, Model showing the role of NANOG during PGCLC induction *in vitro*. D1 EpiLCs are not competent to become PGCLCs, but retain the capability to revert to an ES-like state via 2i LIF and/or *Nanog* overexpression. D2 EpiLCs differentiate into PGCLCs upon *Nanog* expression. NANOG binds to putative enhancer elements of *Prdm1* and *Prdm14* to activate their transcription, which is sufficient to induce the PGCLC fate. This effect can be antagonized by SOX2, which co-binds the *Prdm1* enhancer.

References

31. Yeom, Y. I. *et al.* Germline regulatory element of Oct-4 specific for the totipotent cycle of embryonal cells. *Development* **122**, 881–894 (1996).
32. Yoshimizu, T. *et al.* Germline-specific expression of the Oct-4/green fluorescent protein (GFP) transgene in mice. *Dev. Growth Differ.* **41**, 675–684 (1999).
33. Ying, Q.-L. *et al.* The ground state of embryonic stem cell self-renewal. *Nature* **453**, 519–523 (2008).
34. Schindelin, J. *et al.* Fiji: an open-source platform for biological-image analysis. *Nat. Methods* **9**, 676–682 (2012).
35. Ng, J.-H. *et al.* In vivo epigenomic profiling of germ cells reveals germ cell molecular signatures. *Dev. Cell* **24**, 324–333 (2013).
36. Gillich, A. *et al.* Epiblast stem cell-based system reveals reprogramming synergy of germline factors. *Cell Stem Cell* **10**, 425–439 (2012).
37. Behringer, R., Gertsenstein, M., Nagy, K. V. & Nagy, A. *Manipulating the Mouse Embryo. A Laboratory Manual, 3rd edition*, pp. 453-506 (2003).
38. Cong, L. *et al.* Multiplex genome engineering using CRISPR/Cas systems. *Science* **339**, 819–823 (2013).
39. Marks, H. *et al.* The transcriptional and epigenomic foundations of ground state pluripotency. *Cell* **149**, 590–604 (2012).

Supplementary Table 1: Oligonucleotide sequences

Supplementary Figure 1: Uncropped scans of Western blot gels

Figure 1

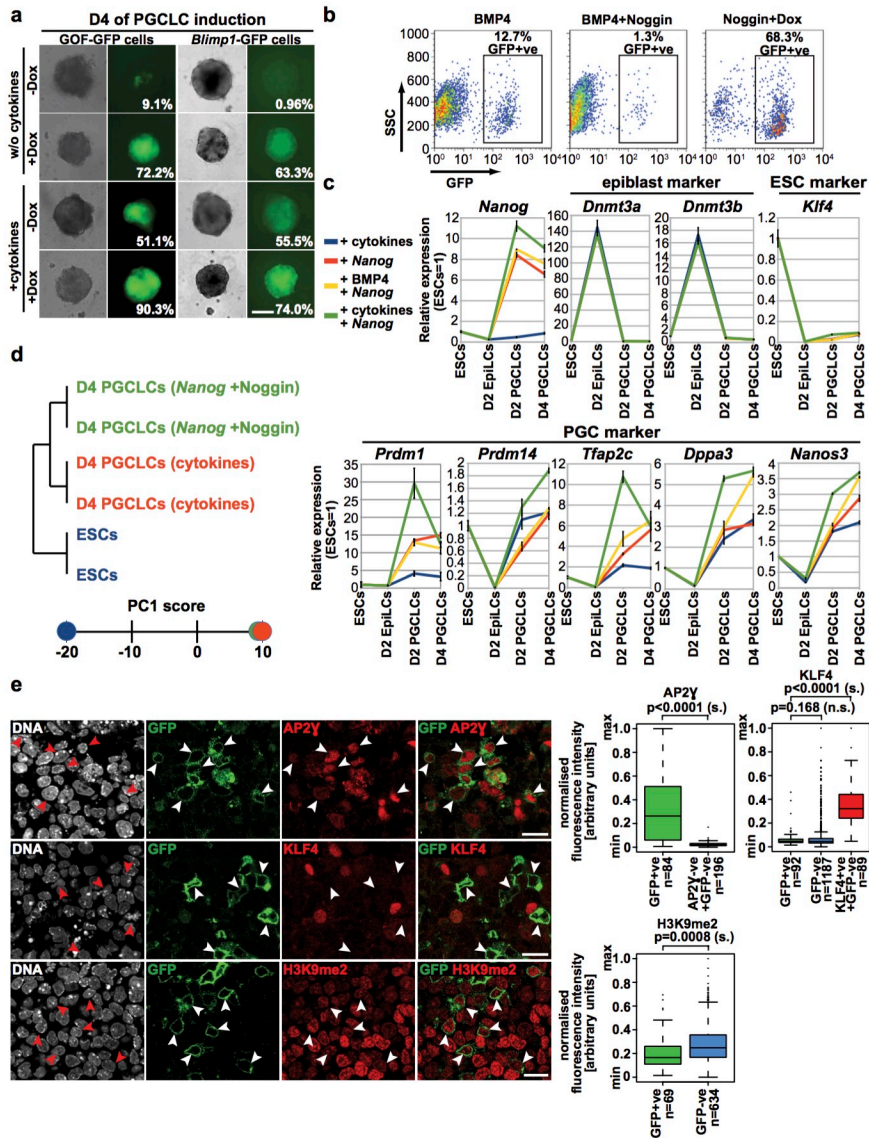


Figure 2

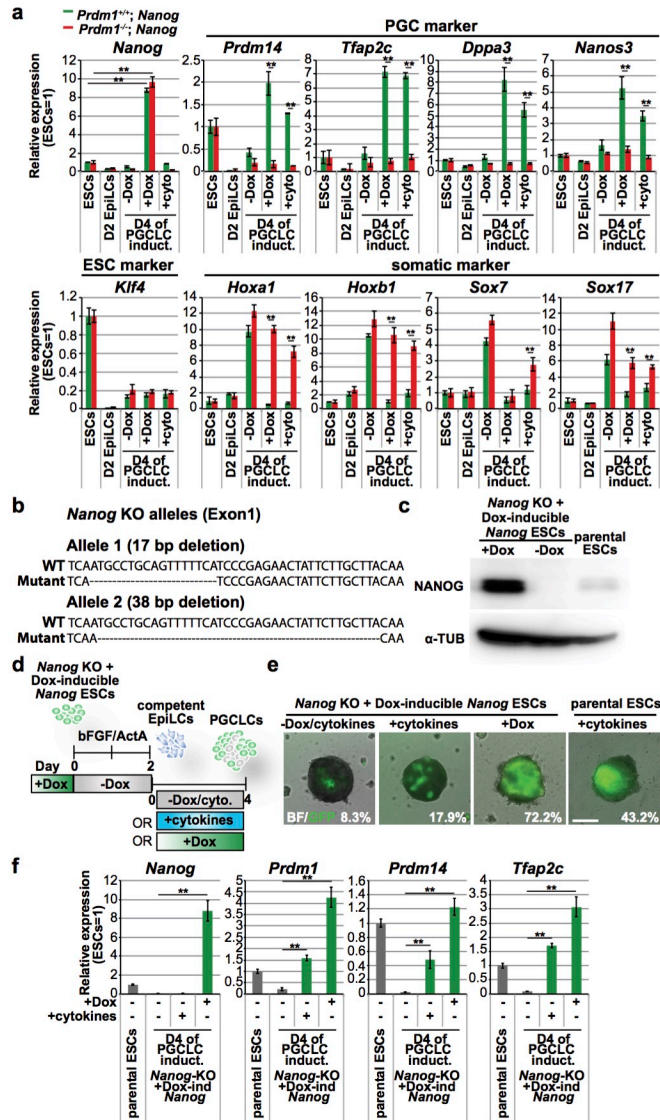


Figure 3

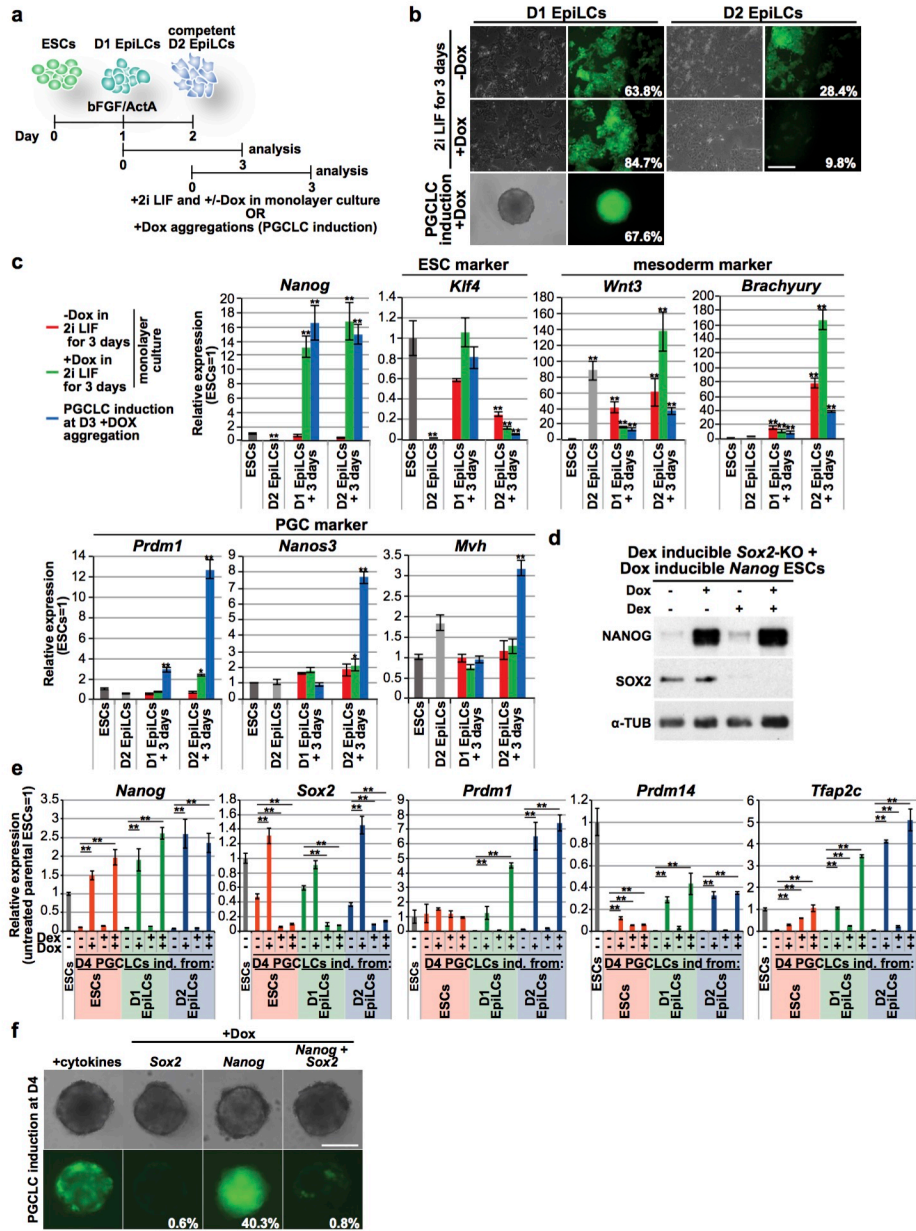
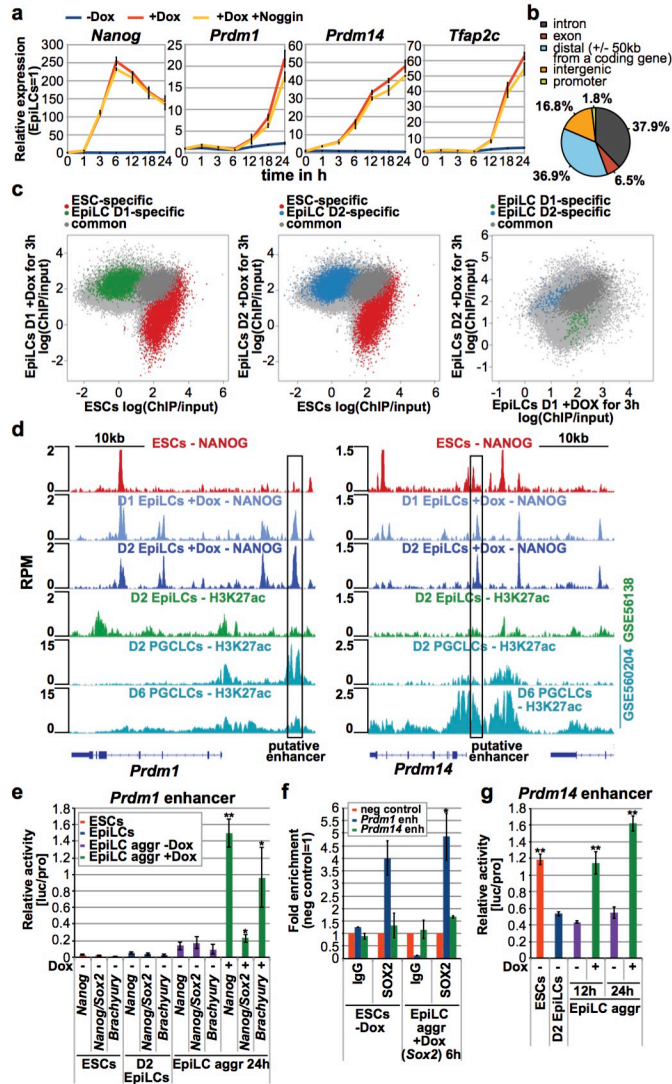
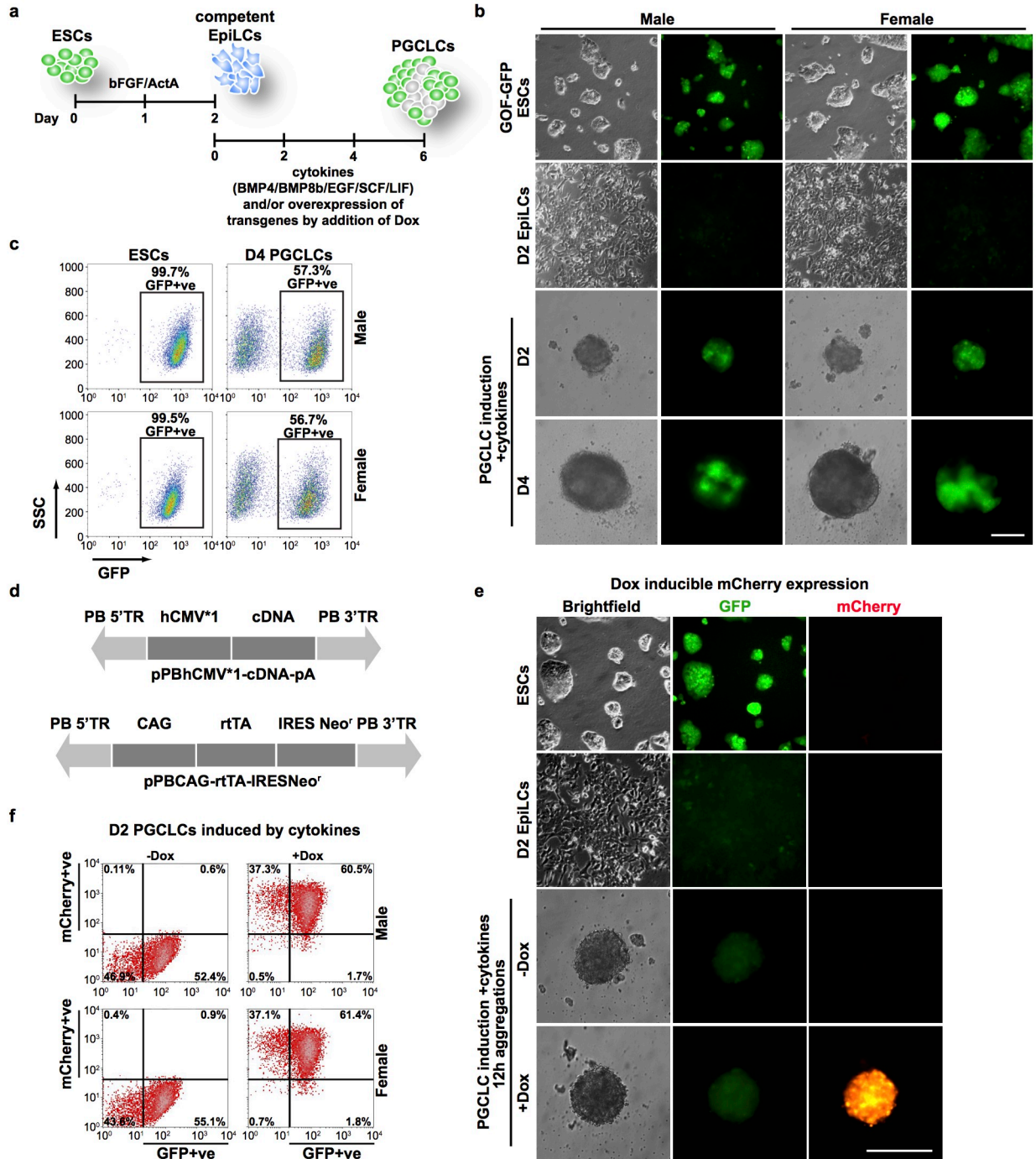


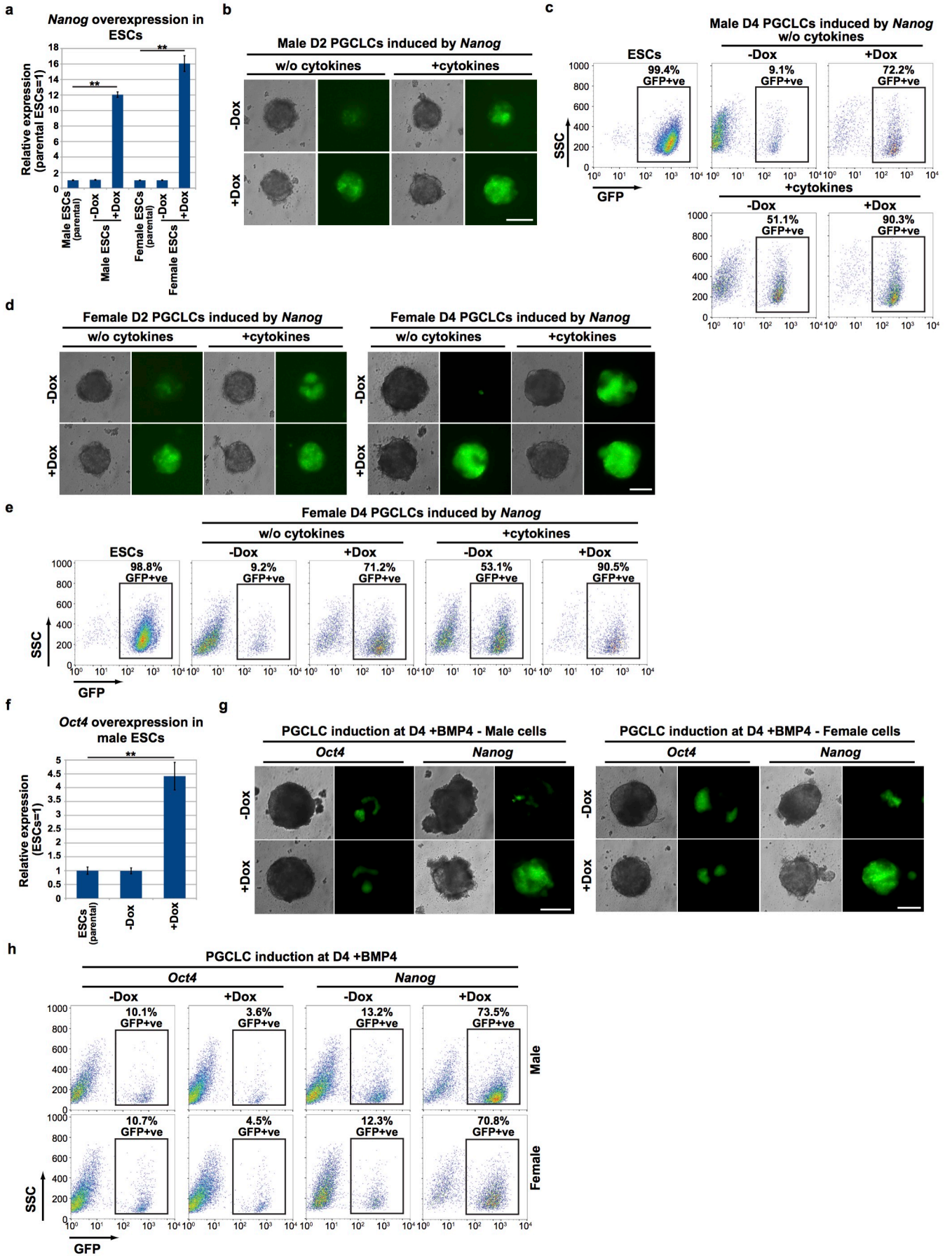
Figure 4



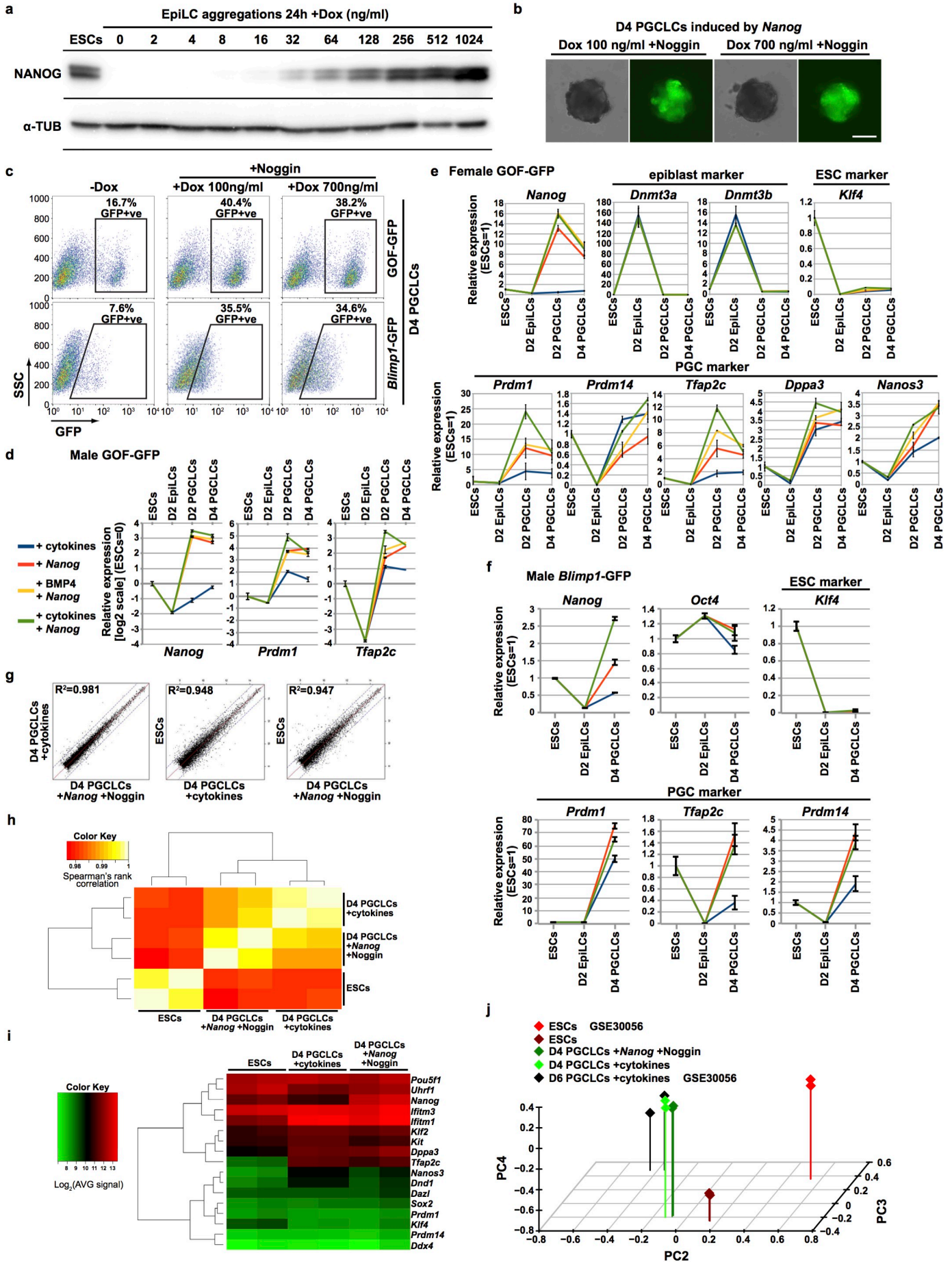
Extended Data Figure 1



Extended Data Figure 2

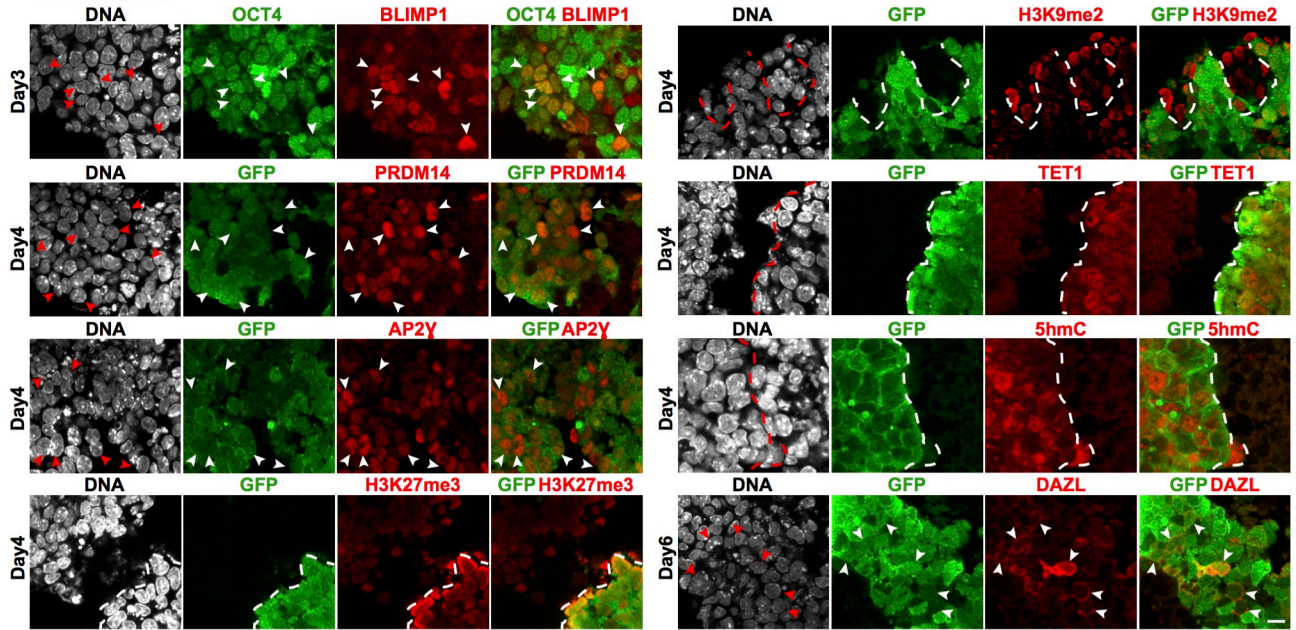


Extended Data Figure 3

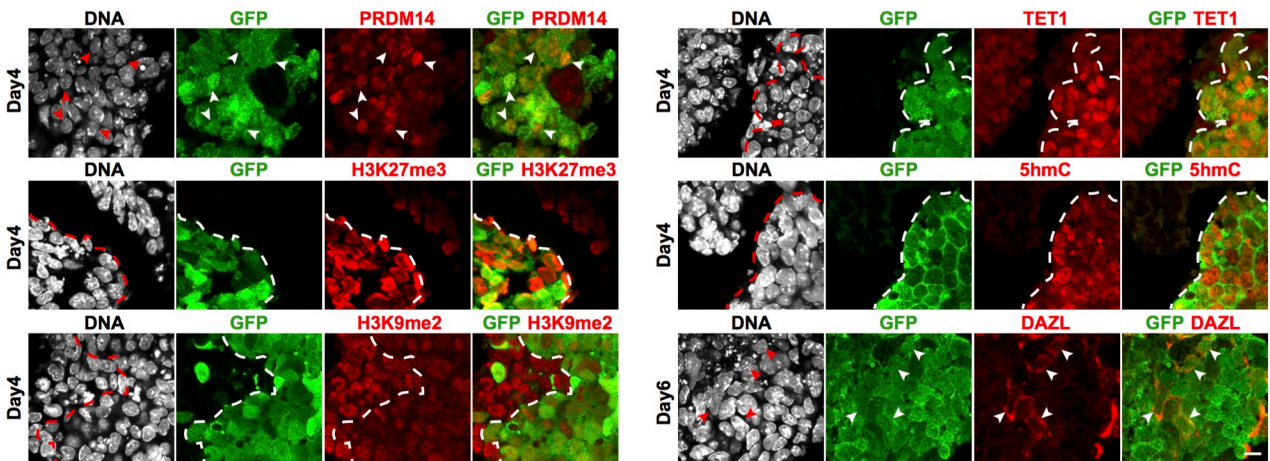


Extended Data Figure 4

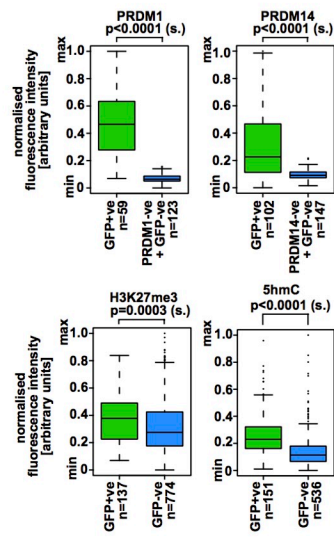
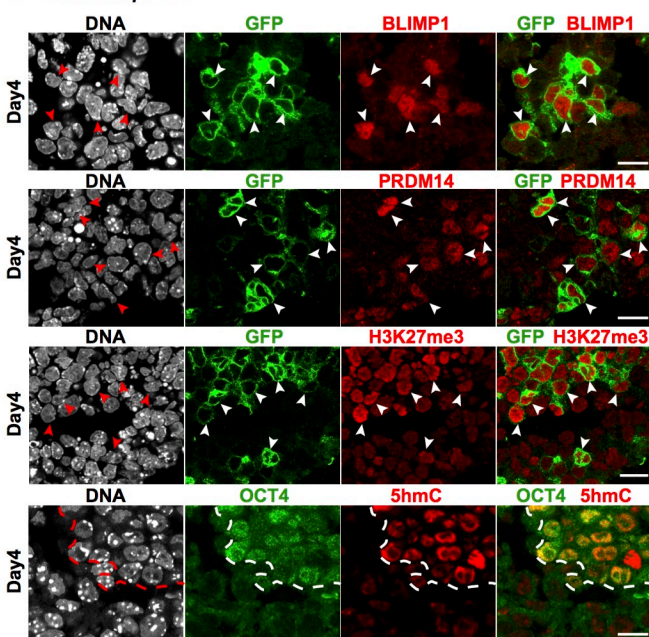
a Male GOF-GFP



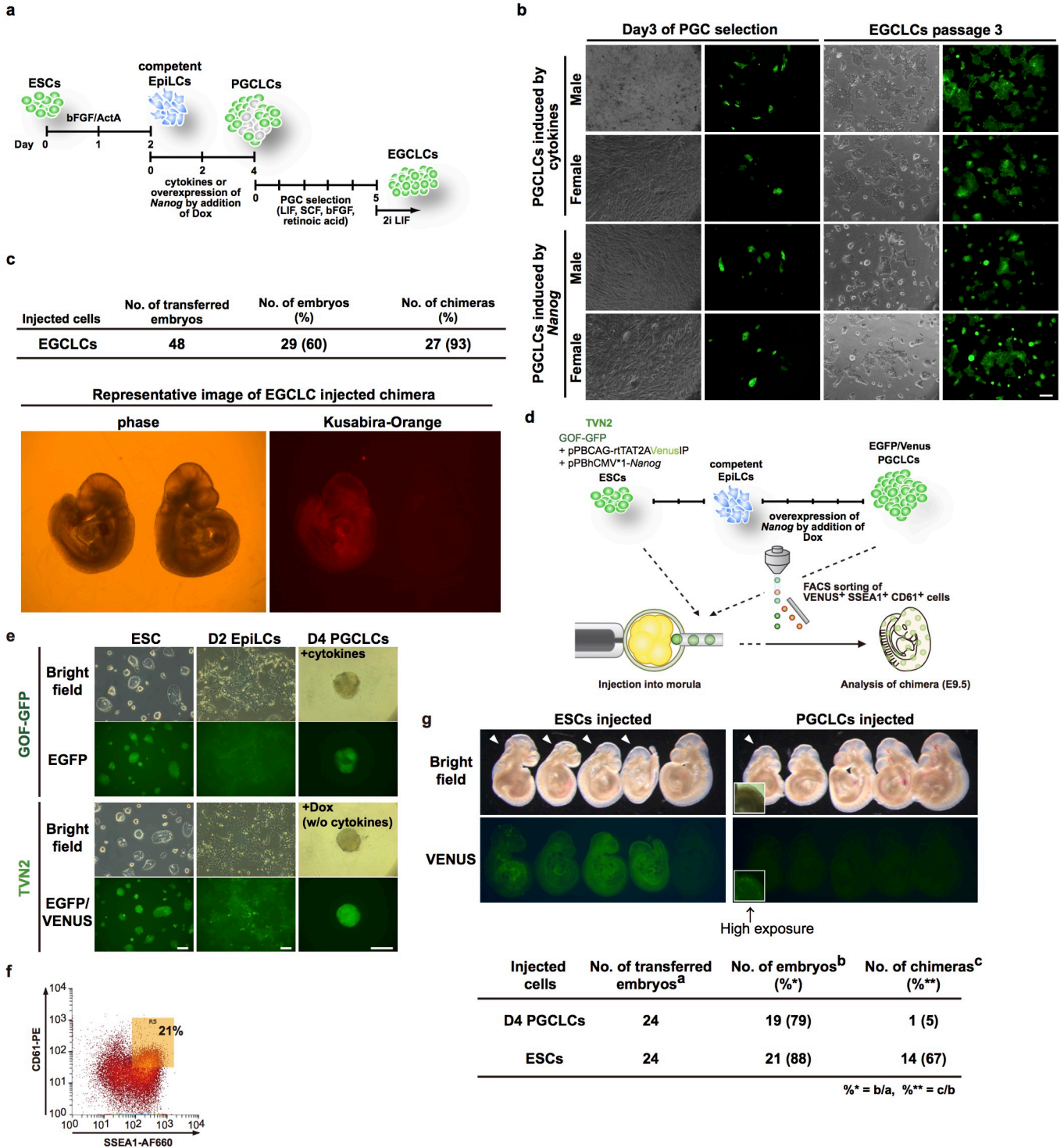
b Female GOF-GFP



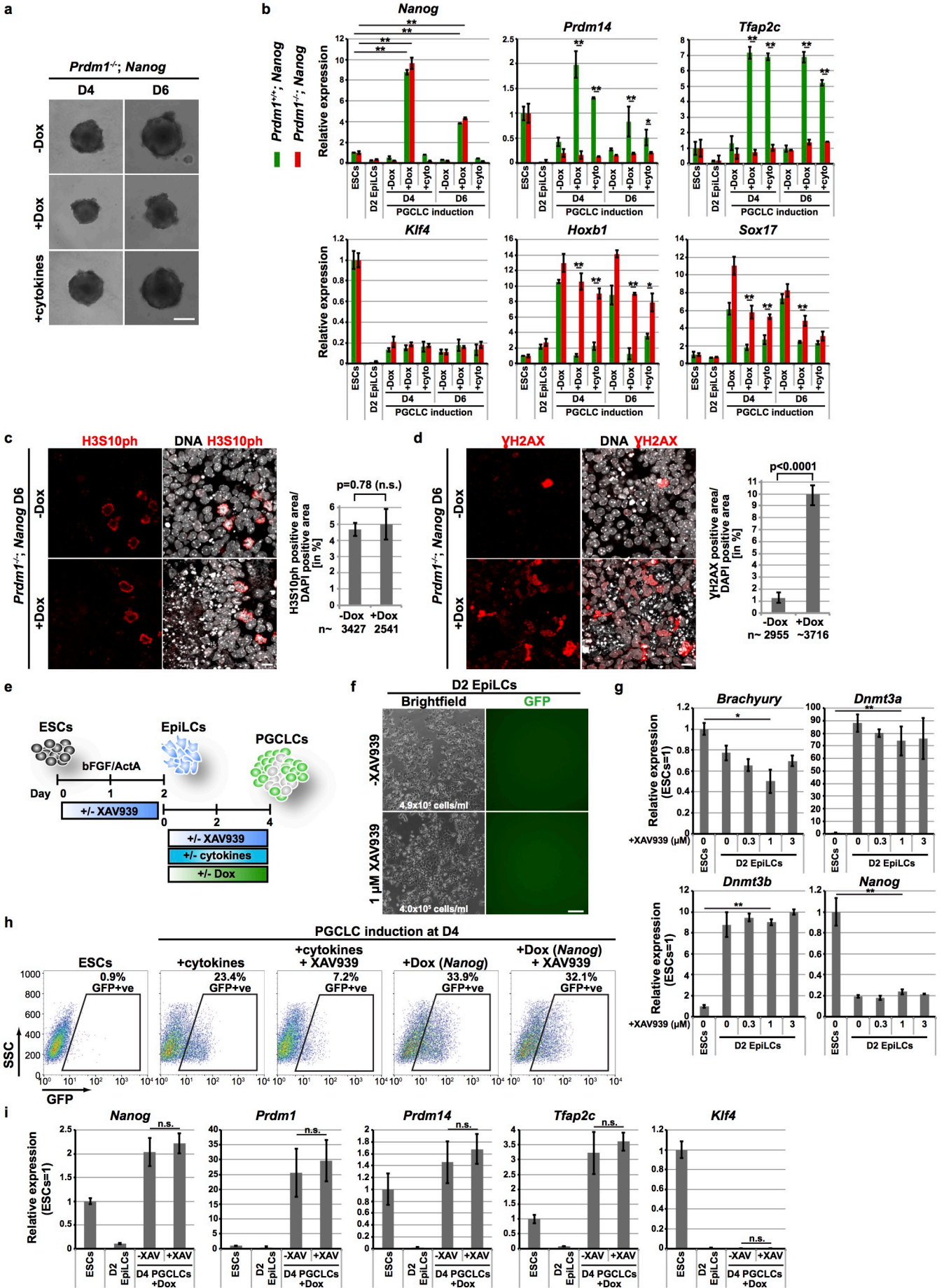
c Male *Blimp1*-GFP



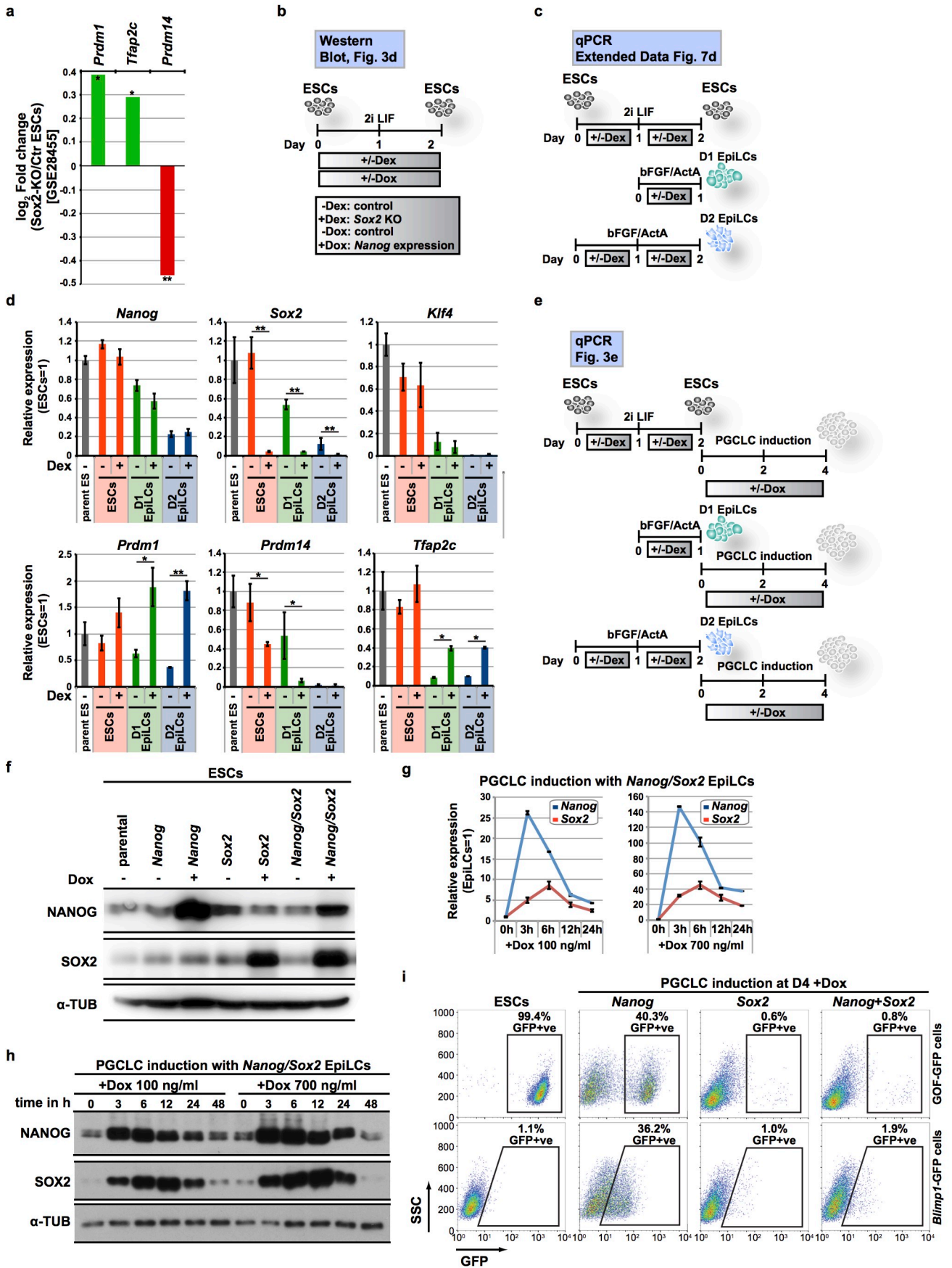
Extended Data Figure 5



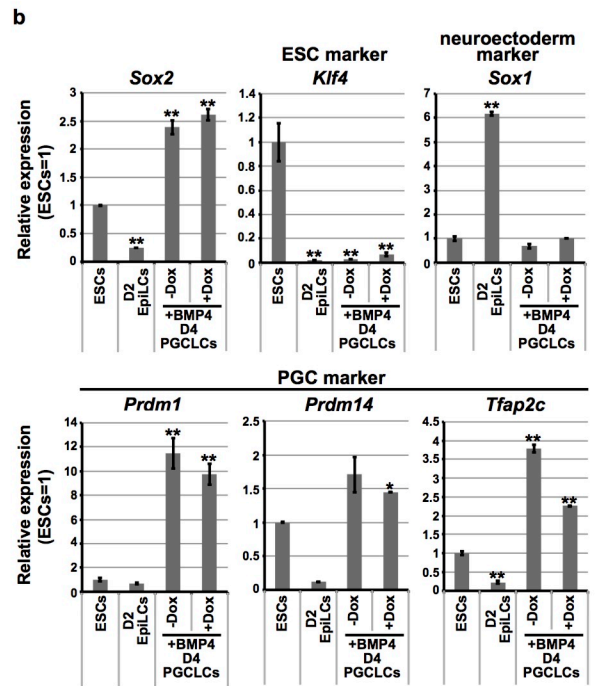
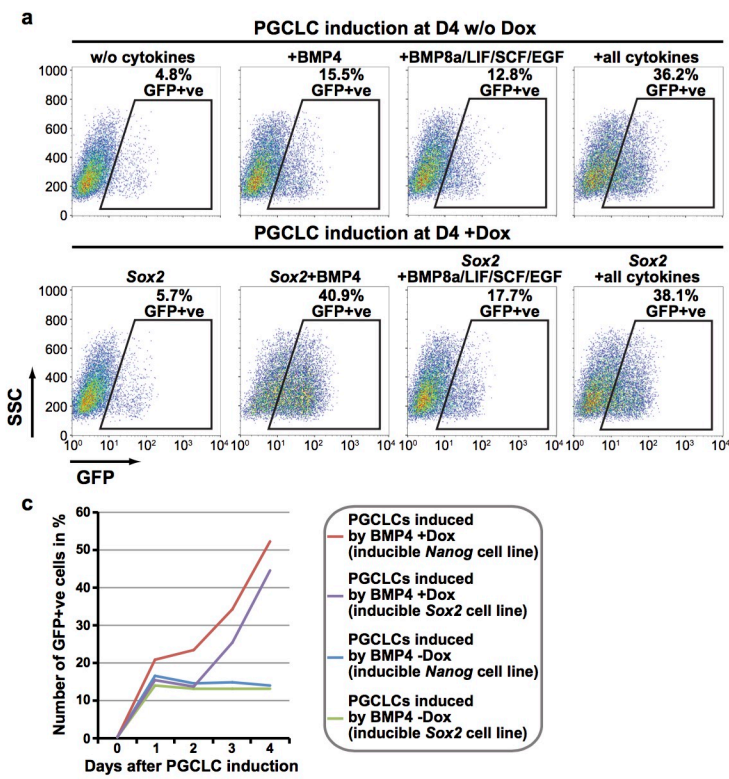
Extended Data Figure 6



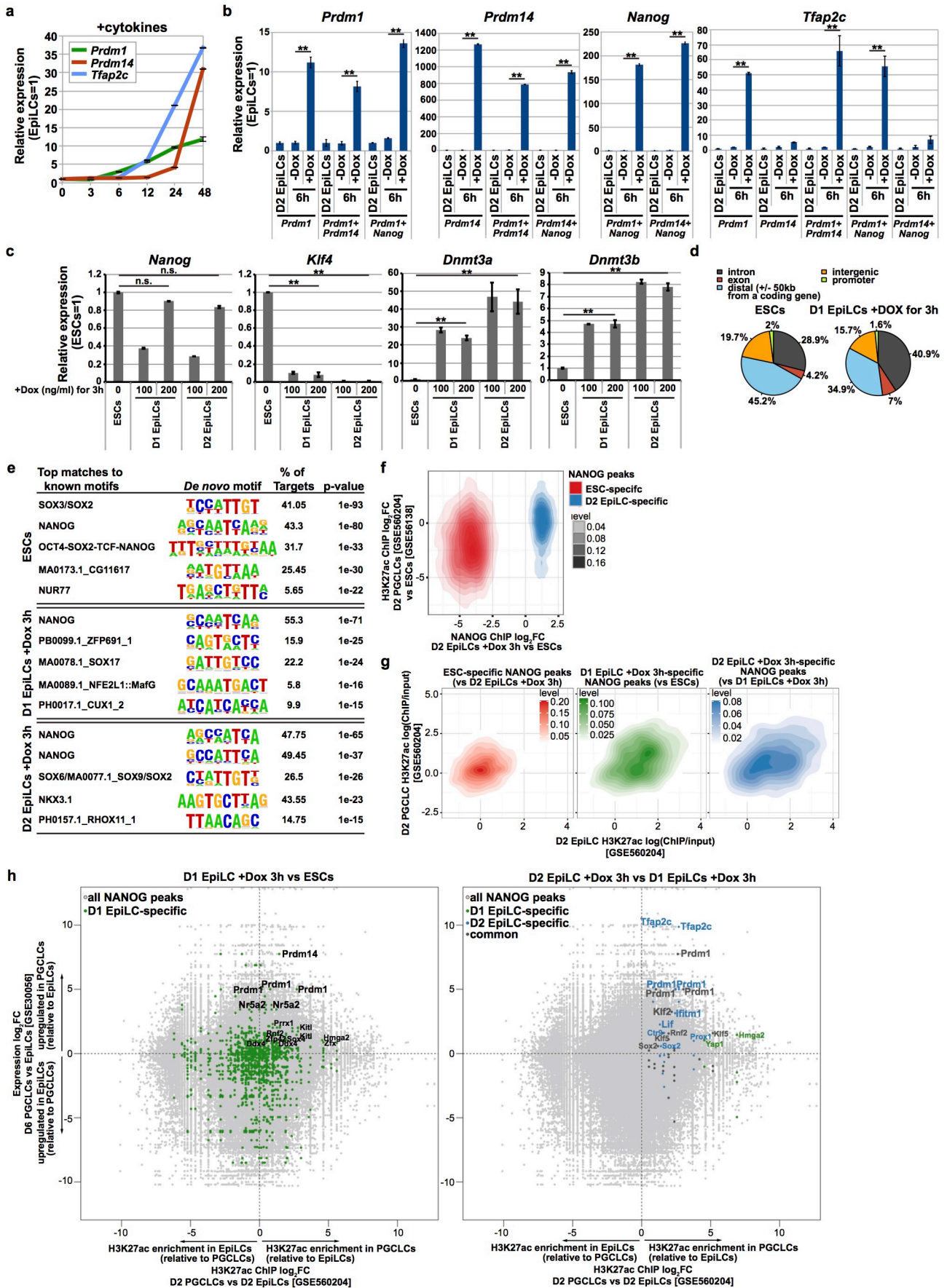
Extended Data Figure 7



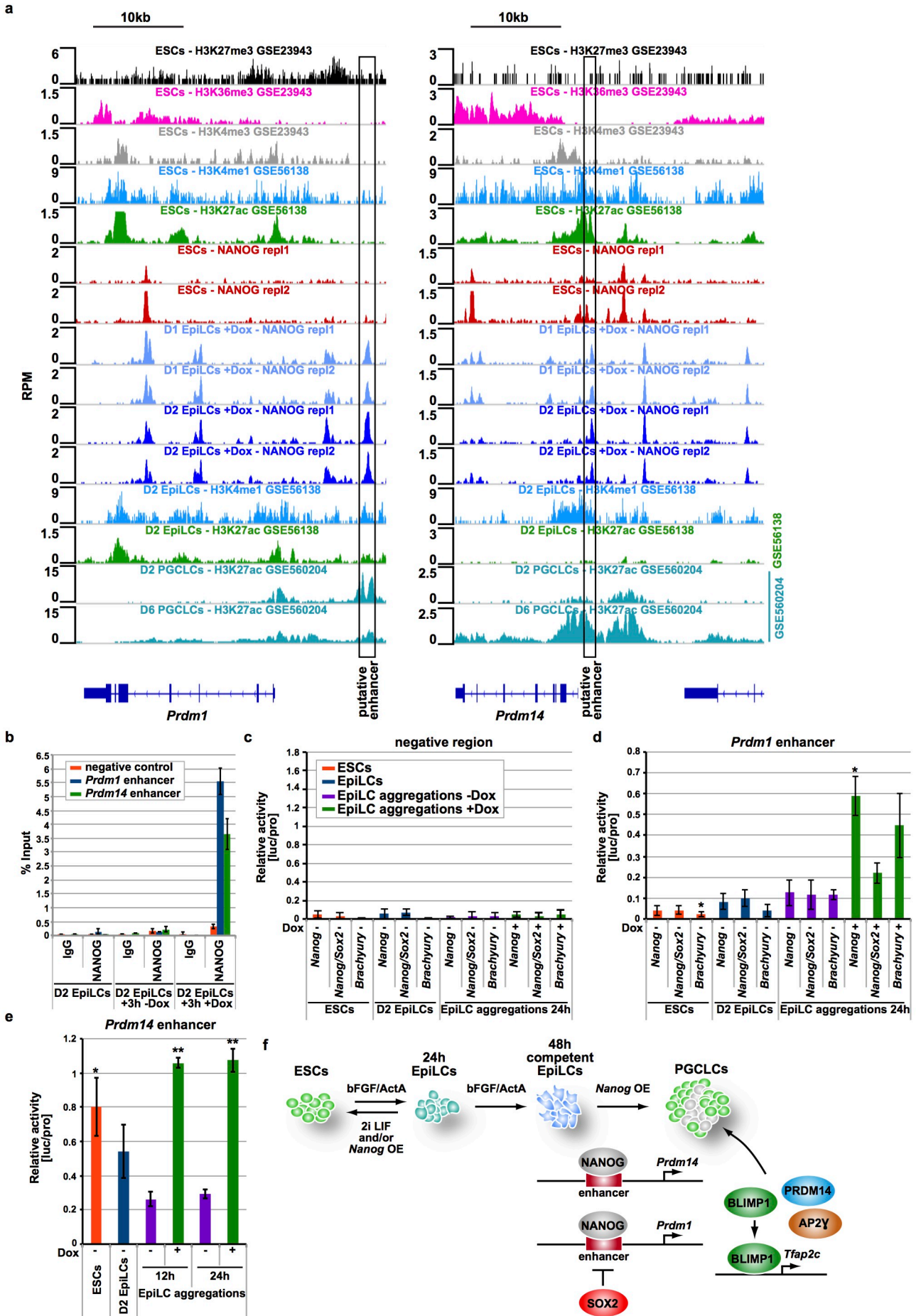
Extended Data Figure 8



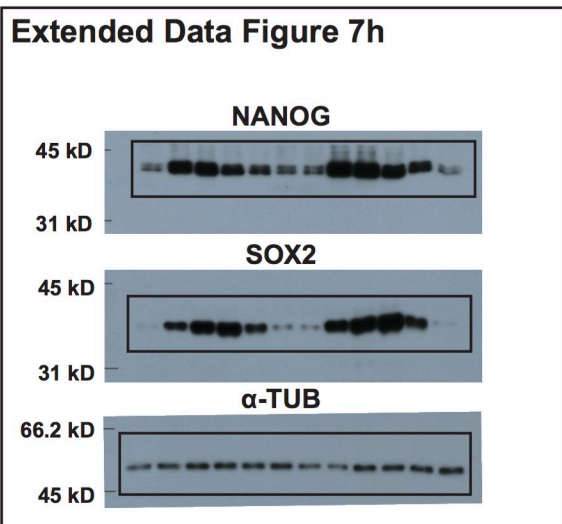
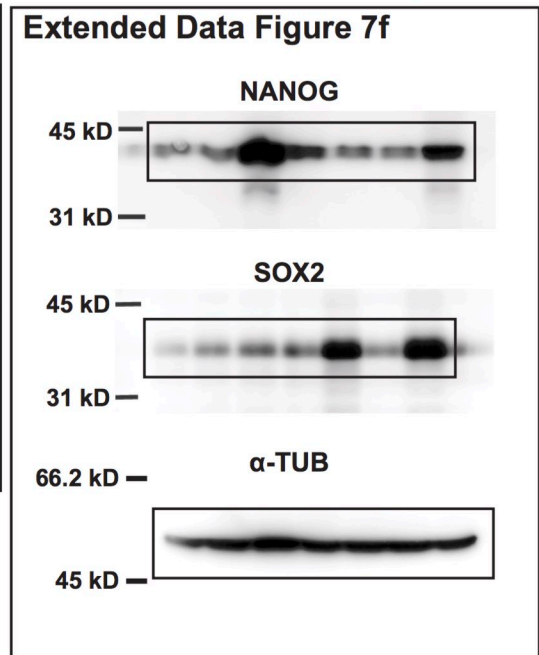
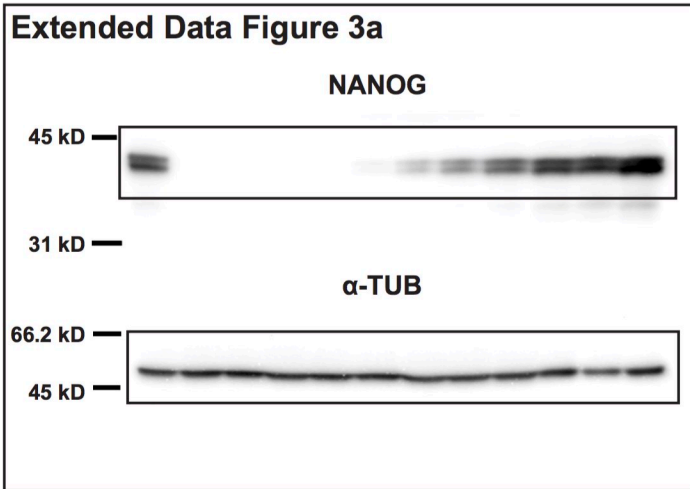
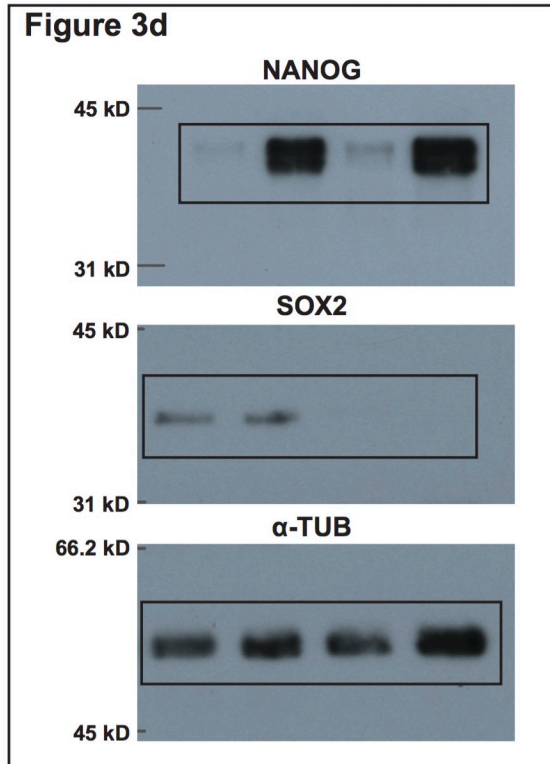
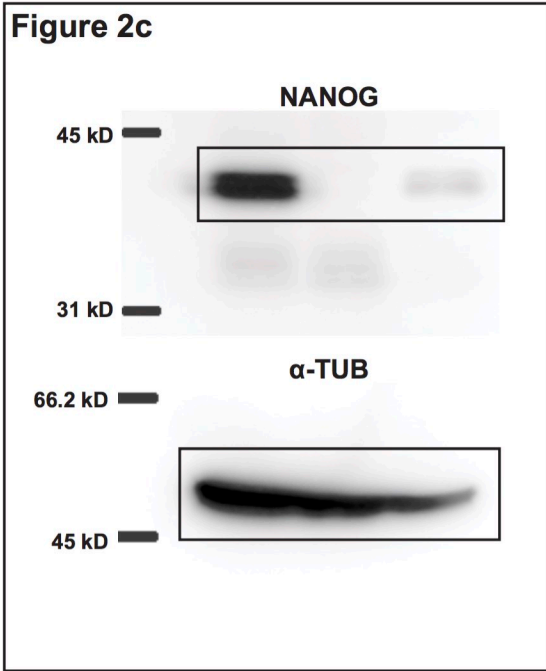
Extended Data Figure 9



Extended Data Figure 10



Supplementary Figure 1: Uncropped scans of Western blot gels



Supplementary Table 1: Oligonucleotide sequences

Gene-specific primers for qRT-PCR

Gene	Forward	Reverse
Gapdh 3'UTR	CCCCAACACTGAGCATCTCC	ATTATGGGGGTCTGGGATGG
Arbp coding	CAAAGCTGAAGCAAAGGAAGAG	AATTAAGCAGGCTGACTTGGTTG
Piap coding	TTACCCATCAAACCATTCTTCTG	AACCCAAAGAACTTCAGTGAGAGC
Oct4 coding	CCAATCAGCTTGGGCTAGAG	CTGGGAAAGGTGTCCCTGTA
Sox2 coding	ACCAGCTCGCAGACCTACAT	TGGAGTGGGAGGAAGAGGTA
Nanog coding	ACCTGAGCTATAAGCAGGTTAAGAC	GTGCTGAGCCCTTCTGAATCAGAC
Klf4 3'UTR	GGGGTCTGATACTGGATGGA	CCCCCAAGCTCACTGATTTA
Prdm1 coding	GAGGATCTGACCCGAATCAA	CATGGAGGTCACATCGACAC
Prdm1 3'UTR	AGCATGACCTGACATTGACACC	CTCAACACTCTCATGTAAGAGGC
Prdm14 coding	GCCTGAACAAGCACATGAGA	TGCACTTGAAGGGCTTCTCT
Prdm14 3'UTR	ACAGCCAAGCAATTTGCACTAC	TTACCTGGCATTTCATTGCTC
Tfap2c coding	ATCAAGATCGGACACCCAAC	ATGGCGATTAGAGCCTCCTT
Tfap2c 3'UTR	TGAAGATGAAGCTGGGCTTT	TCCATTCTCTTCCGTTTCAG
Dppa3 coding	AGGCTCGAAGGAAATGAGTTTG	TCCTAATTCTTCCCGATTTTCG
Nanos3 coding	CACTACGGCCTAGGAGCTTGG	TGATCGCTGACAAGACTGTGG
Mvh 3'UTR	CAGTTTGCAATGTGAGCTTTG	GGGGGAAATGTGTTTCATCTT
Wnt3 coding	CAAGCACACAATGAAGCAGGC	TCGGGACTCACGGTGTTCCTC
Brachyury 3'UTR	ATCAGAGTCCTTTGCTAGGTAG	GTTACAATCTTCTGGCTATGC
Dnmt3a 3'UTR	GACTCGCGTGCAATAACCTTAG	GGTCACTTCCCTCACTCTGG
Dnmt3b coding	CTCGCAAGGTGTGGGCTTTTGTAAC	CTGGGCATCTGTCATCTTTGCACC
Hoxa1 3'UTR	GTGACTAGTCTTCTGCATGTCG	TCTGCTCTGGACCACATCACTC
Hoxb1 3'UTR	GATCCTACAGGTCTTGGGACC	AGCTCAAAGGCACTGAACTGAG
Sox1 3'UTR	CCTGTGGTTCTGCCTTTTGC	TGAGCACAACCCATCCTCCT
Sox7 3'UTR	CCACAGTCCTTTGGCTGTCC	TACACGTGTCCAAGGGCAGA
Sox17 3'UTR	TTCTGTACACTTTAATGAGGCTGTTC	TTGTGGGAAGTGGGATCAAG

gRNA sequences for Nanog knockout

Target	Top	Bottom
Nanog exon1	CACCGTTCTCGGGATGAAAACTGC	AAACGCAGTTTTTTCATCCCGAGAAC

Primers for chromatin immunoprecipitation

Amplified region	Forward	Reverse
Negative control	AGGAGACCAGAGAGGCAAGA	GTCTTGAGGCCAGAAACCTC
Prdm1 enhancer	GCATCAGGAGATTGCCCTT	GCTGTGTGAGGTCCTCTGTG
Prdm14 enhancer	TCAAAGAAAGGGGTGAGCTT	TCAAAGAAAGGGGTGAGCTT

Primers for cloning of putative enhancers

Putative enhancer	Top	Bottom
Prdm1	GAGGATCAGGAGTTCAAGTTGGCTA	GGGGCAAACAGGTGAGTTTATTATT
Prdm14	CCCTCACACACACTACACCC	AGCAACTGGAAGACTGAGGC